

Internal Alkyne Isomerization to Vinylidene versus Stable π -Alkyne: Theoretical and Experimental Study on the Divergence of Analogous Cp^*Ru and TpRu Systems

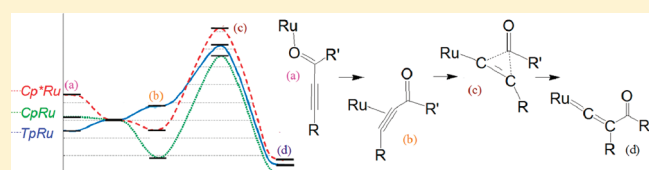
Vinay K. Singh,[†] Emilio Bustelo,[†] Isaac de los Ríos,[†] Ignacio Macías-Arce,[†] M. Carmen Puerta,^{*,†} Pedro Valerga,^{*,†} Manuel Ángel Ortuño,[‡] Gregori Ujaque,[‡] and Agustí Lledós^{*,‡}

[†]Departamento de Ciencia de los Materiales e Ingeniería Metalúrgica y Química Inorgánica, Facultad de Ciencias, Universidad de Cádiz, 11510 Puerto Real (Cádiz), Spain

[‡]Departament de Química, Universitat Autònoma de Barcelona, 08193 Bellaterra, Barcelona, Spain

S Supporting Information

ABSTRACT: The activation of internal alkynes by Cp^*Ru and TpRu complexes gives respectively π -alkyne and disubstituted vinylidene as stable species, even though both systems bear identical pyridylphosphine ligands ($\kappa^2\text{-P,N-}^i\text{Pr}_2\text{PXPpy}$, X = NH, CH_2 , S). The activation of the alkynes $\text{PhC}\equiv\text{CCOR}$ (R = Me, Ph) by $[\text{TpRuCl}(\text{}^i\text{Pr}_2\text{PXPpy})]$ complexes allowed us to isolate and characterize metastable $\eta^1\text{-O=C(R)C}\equiv\text{CPh}$ adducts. These complexes isomerize spontaneously to vinylidene both in solution and in the solid state. Kinetic studies have been carried out in solution by $^{31}\text{P}\{^1\text{H}\}$ NMR and in the solid state by IR spectroscopy, providing the Eyring and Avrami–Erofeev parameters, respectively. The activation of internal alkynes without ketone groups provided vinylidene species as well, but without isolable intermediates. In contrast with the TpRu system, the activation of alkynes by $[\text{Cp}^*\text{RuCl}(\text{}^i\text{Pr}_2\text{PXPpy})]$ always results in stable π -alkyne species. Representatives of both $\text{Cp}^*\text{Ru}-\pi$ -alkyne and TpRu -vinylidene compounds have been characterized by X-ray diffraction. DFT calculations have been carried out with the actual experimental complexes, including solvent effects, in order to analyze the mechanism of the π -alkyne to vinylidene isomerization of internal alkynes and to explain the divergent results obtained for Tp and Cp^* .



INTRODUCTION

It is well-known that the relative stability of alkyne and vinylidene isomers is reversed upon coordination to a variety of transition metals. This process ($\text{HC}\equiv\text{CR} \rightarrow \text{:C=CHR}$) is the main synthetic route to vinylidene species^{1,2} and is a key step for several catalytic alkyne transformations.³ The simplest role of the metal is to stabilize the vinylidene lone pair of electrons by means of a dative carbon→metal bond, throughout a concerted 1,2-H rearrangement. A stronger participation of the metal involves the oxidative addition of the alkyne to yield alkynyl–hydride intermediates, followed by a formal 1,3-H migration. The nature and pathway of the migrating hydrogen have been the objects of numerous theoretical studies.⁴ The concerted 1,2-H shift is predominant in ruthenium chemistry, with the remarkable exception of some electron-rich complexes such as $[\text{Cp}^*\text{Ru}(\text{L})(\text{PEt}_3)_2][\text{BAR}^{\text{F}}_4]$, for which the full sequence of intermediates was isolated and characterized by X-ray diffraction (π -alkyne/alkynyl–hydride/vinylidene).⁵

The π -coordination of the alkyne to the metal is generally accepted as the first mechanistic step, but both electronic and steric factors contribute to favor the spontaneous rearrangement to the linear vinylidene chain. The higher thermodynamic stability of the vinylidene ligand is mainly explained by its better

π -acceptor capability with respect to the π -alkyne isomer. As a general rule, the relative vinylidene stability will increase with the electron density on the metal center, particularly with the presence of stronger (and bulkier) donor ligands in the metal coordination sphere. This is the case of the numerous examples of stable vinylidene complexes of the type $[\text{Cp}^*\text{Ru}(\text{=C=CHR})(\text{PR}_3)_2]^+$.⁶ In contrast, electron-poor dicarbonyl systems such as $[\text{CpFe}(\text{CO})_2(\text{=C=CRR}')^+]$ (R, R' = Me, Ph) spontaneously undergo isomerization to π -alkyne complexes.⁷ Intermediate situations have led to the observation of vinylidene/ π -alkyne equilibria^{4e} and to reversible alkyne/vinylidene isomerization, which is essential for several catalytic reactions via vinylidene intermediates.¹

The conversion of internal alkynes to vinylidenes ($\text{RC}\equiv\text{CR}' \rightarrow \text{:C=CRR}'$) is a quite uncommon process that has just emerged during the last few years as a new promising route for the transformation of internal alkynes via vinylidene intermediates.² Earlier, this process had only been reported for a series of heteroatom-substituted alkynes, namely alkynylsilanes,⁸ tin acetylides,⁹ 1-iodo-1-alkynes,¹⁰ and mercaptoacetylene.¹¹ In

Received: March 28, 2011

Published: July 05, 2011

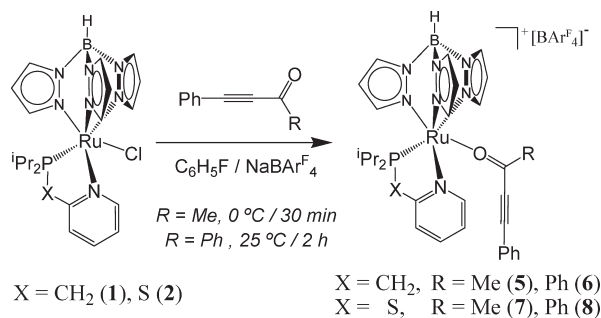
Scheme 1. Synthesis of TpRu- η^1 -Ketone Adducts

Table 1. Selected IR (Nujol, cm^{-1}) and $^{31}\text{P}\{^1\text{H}\}$ and $^{13}\text{C}\{^1\text{H}\}$ NMR Data (δ) for Compounds 5–8 and the Free Alkynyl Ketones

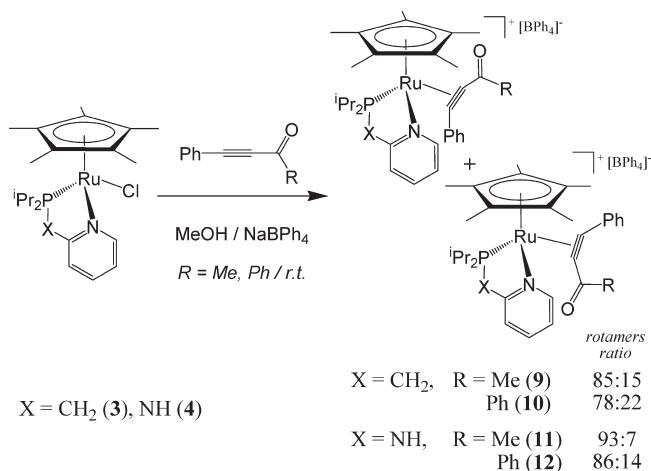
compd	$\nu(\text{C}\equiv\text{C})$	$^{31}\text{P}\{^1\text{H}\}$	$^{13}\text{C}\{^1\text{H}\}$	
			$\text{C}\equiv\text{C}$	$\text{C}=\text{O}$
4-phenyl-3-butyn-2-one	2203, 2126 ^a		88.9, 90.0	184.1
1,3-diphenylpropynone	2200		87.2, 95.7	178.5
5	2204, 2160 ^a	71.7	87.4, 106.7	198.3
6	2196	71.5	85.9, 106.3	189.7
7	2203, 2159 ^a	139.5	87.4, 107.8	198.5
8	2188	139.5	86.0, 107.5	189.7

^a A weak, broad shoulder is observed beside the main peak.

recent times, the migration of carbon substituents has been shown to be possible, opening a novel access to disubstituted vinylidenes from internal alkynes.

The first example reported the formation of bridging vinylidene species by activation of acetylenedicarboxylate within a binuclear ruthenium complex.¹² More recently, Shaw et al. have described that internal alkynes, $\text{RC}\equiv\text{CCOR}'$, are also transformed into their isomeric disubstituted vinylidenes by $[\text{CpRuCl}(\text{PPh}_3)_2]$.¹³ A ruthenium cyclophosphane complex is able to reproduce this behavior with aryl-, alkyl-, and carboxy-substituted internal alkynes, establishing their relative migratory aptitude and providing the first mechanistic insight.¹⁴ Aryl- and alkyl-disubstituted vinylidenes have also been obtained by reaction of $[\text{CpRu}(\text{dppe})\text{Cl}]$ and $[\text{CpFe}(\text{dppe})\text{Cl}]$ with $\text{PhC}\equiv\text{CAr}$ ($\text{Ar} = p\text{-C}_6\text{H}_4\text{X}$; $\text{X} = \text{OMe}, \text{Me}, \text{H}, \text{Cl}, \text{COOEt}$) and 2-pentyne.¹⁵ Finally, the reverse process (vinylidene to π -alkyne isomerization) has been reported for the aforementioned electrophilic iron complexes.⁷ From these studies the migratory aptitude of the alkyne substituents have been disclosed, electron-withdrawing groups increasing the migratory aptitude in the order $\text{CO}_2\text{Et} \approx \text{C}_6\text{H}_4\text{-CO}_2\text{Et-}p > \text{Me} > \text{Ph} > \text{C}_6\text{H}_4\text{-Me-}p > \text{C}_6\text{H}_4\text{-OMe-}p$.^{2,14,15}

An important issue regarding the scope of the conversion of internal alkynes into their corresponding vinylidene ligands and its potential exploitation in synthetic chemistry is assessment of the influence of the transition-metal ligands in the transformation. Most of the complexes able to perform such processes are half-sandwich ruthenium complexes with Cp-related ligands, and a natural extension is to check the behavior of tris(pyrazolyl)borate (Tp) ligands. Comparisons between Cp- and Tp-type ligands can be found regarding H_2 ¹⁶ and C-H ¹⁷ activation. In

Scheme 2. Synthesis of Cp*Ru- π -Alkynone Complexes

our first contribution to this field, we showed that TpRu complexes can also effect the alkyne to vinylidene isomerization in internal alkynes.¹⁸ In agreement with Shaw's results, we were able to isolate the η^1 -ketone-bound alkynone complexes as the kinetic products, which then undergo isomerization to the vinylidene form, both in solution and in the solid state. The kinetic studies on this transformation support the existence of an intramolecular process, and a concerted 1,2-acyl migration is proposed as the key step. Although the presence of π -alkyne species during the isomerization process can be reasonably proposed on the basis of the $^{31}\text{P}\{^1\text{H}\}$ NMR and IR monitoring of the reaction, their role as actual intermediates of the process is not yet clear.

This paper is aimed at comparing the behavior of Tp- and Cp*-ruthenium complexes to facilitate the conversion of internal alkynes into their vinylidene isomers. We extend our previous results on $[\text{TpRu}(\text{P}^i\text{Pr}_2\text{Me})(\text{MeCN})]^+$ and $[\text{TpRu}(\kappa^2\text{P}, \text{N}^i\text{Pr}_2\text{PNHPy})]^+$ to the related $[\text{TpRu}(\kappa^2\text{P}, \text{N}^i\text{Pr}_2\text{PCH}_2\text{Py})]^+$ and $[\text{TpRu}(\kappa^2\text{P}, \text{N}^i\text{Pr}_2\text{PSPy})]^+$ fragments, in order to assess the effect of the pyridylphosphine spacer group (NH, CH₂, S) on the isomerization process, supported by kinetic studies providing the Eyring plots and activation parameters. The use of P,N-donor ligands adds additional interest to this research because of their potential hemilabile character,¹⁹ which in the future might allow the development of stoichiometric and catalytic transformation of internal alkynes. Disubstituted vinylidenes have also been obtained starting from internal alkynes not bearing a ketone group: $\text{RC}\equiv\text{CR}'$ (R, R' : Ph, COOMe; Me, COOEt; Ph, Ph).

Finally, the related complexes $[\text{Cp}^*\text{RuCl}(\kappa^2\text{P}, \text{N}^i\text{Pr}_2\text{PXPpy})]$ ($\text{X} = \text{NH}, \text{CH}_2$) have been tested in the activation of internal alkynes, isolating and characterizing π -alkyne complexes as stable products, which resist isomerization to vinylidene even at high temperatures and long reaction times. X-ray structures have been determined for the compounds $[\text{Cp}^*\text{RuCl}(\kappa^2\text{P}, \text{N}^i\text{Pr}_2\text{PSPy})]$, $[\text{Cp}^*\text{Ru}(\eta^2\text{-PhC}\equiv\text{CCOPh})(\kappa^2\text{P}, \text{N}^i\text{Pr}_2\text{PNHPy})]$, $[\text{TpRu}\{\text{C}=\text{C}(\text{COMe})\text{Ph}\}(\kappa^2\text{P}, \text{N}^i\text{Pr}_2\text{PSPy})][\text{BAR}^F_4]$, and $[\text{TpRu}\{\text{C}=\text{C}(\text{COOMe})\text{Ph}\}(\kappa^2\text{P}, \text{N}^i\text{Pr}_2\text{PCH}_2\text{Py})][\text{BAR}^F_4]$.

The two related ruthenium complexes differ only in the presence of a Tp or Cp* ligand yet exhibit contrasting behavior regarding the isomerization of the same internal alkyne to vinylidene. This finding makes these complexes very appealing for analysis of the factors which control this process. With the

Table 2. Selected IR (Nujol, cm^{-1}) and $^{31}\text{P}\{^1\text{H}\}$ and $^{13}\text{C}\{^1\text{H}\}$ NMR Data (δ) for 9–12, 19, and 20

	$\nu(\text{C}\equiv\text{C})$	$^{31}\text{P}\{^1\text{H}\}$	$^{13}\text{C}\{^1\text{H}\}$	
			$\text{C}\equiv\text{C}$	$\text{C}=\text{O}$
9	1828	66.4 (s, 15%)	86.10 (d, 9.6 Hz) ^a	190.9 (s) ^a
		69.8 (s, 85%) ^a	116.8 (d, 4.8 Hz) ^a	
10	1800	66.8 (s, 22%)	85.02 (d, 8.8 Hz) ^a	185.3 (d, 3.8 Hz) ^a
		68.3 (s, 78%) ^a	113.4 (d, 5.0 Hz) ^a	
11	1842	128.0 (s, 7%)	84.59 (d, 9.2 Hz) ^a	190.2 (s) ^a
		128.3 (s, 93%) ^a	115.7 (br s) ^a	
12	1871	126.9 (s, 86%) ^a	85.15 (d, 8.3 Hz) ^a	185.4 (d, 3.8 Hz) ^a
		127.3 (s, 14%)	114.2 (d, 4.5 Hz) ^a	
19	1842	67.2 (s, 40%) ^b	87.02 (s)/94.19 (s) ^b	159.0 (d, 3.8 Hz) ^b
		69.8 (s, 60%) ^b	82.23 (s)/92.81 (s) ^b	158.6 (d, 3.8 Hz) ^b
20	1856	127.7 (s, 45%) ^c	76.90 (d, 9.7 Hz) ^c	162.3 (d, 4.8 Hz) ^c
		127.9 (s, 55%) ^c	105.9 (d, 4.6 Hz) ^c	163.0 (s) ^c
			78.33 (d, 5.6 Hz) ^c	
			102.1 (d, 9.8 Hz) ^c	

^a $^{13}\text{C}\{^1\text{H}\}$ NMR data correspond to the major rotamer. ^b $^{13}\text{C}\{^1\text{H}\}$ NMR signals are clearly identifiable and assignable to each rotamer. ^c $^{13}\text{C}\{^1\text{H}\}$ NMR signal assignment to rotamers is ambiguous and exchangeable.

goal of unraveling the mechanistic features of the isomerization of internal alkynes and justifying the contradictory results obtained for Tp and Cp* ruthenium complexes, we have performed DFT calculations that are also collected in this article.

RESULTS AND DISCUSSION

Experimental Results on the Activation of Internal Alkynes. Hydrotris(pyrazolyl)borate (Tp) and pentamethylcyclopentadienyl (Cp*) are isoelectronic ligands widely employed in organometallic chemistry and catalysis. Both polydentate ligands are able to block three coordination sites on a metal center, giving rise to a large family of compounds with three-legged piano-stool geometries. In spite of their obvious similarities, the Cp* derivatives are usually considered to be more electron rich than the Tp analogues, and the increased donation of the Cp* ligand to the metal results in a greater π back-bonding when suitable π -acceptor ligands are present.

Consequently, the chloride abstraction process is much harder for the TpRu starting complexes [TpRuCl($\kappa^2\text{P},\text{N}^1\text{Pr}_2\text{XPy}$)] ($\text{X} = \text{CH}_2$ (1), S (2)); the process is only possible in the presence of NaBAR₄^F (Ar^F = 3,5-bis(trifluoromethyl)phenyl). On the other hand, the Cp*Ru derivatives [Cp*RuCl($\kappa^2\text{P},\text{N}^1\text{Pr}_2\text{XPy}$)] ($\text{X} = \text{CH}_2$ (3), NH (4)) can release the halide spontaneously in methanol solution. Thus, NaBPh₄ has been employed instead of NaBAR₄^F for practical reasons. The use of NaBAR₄^F in Cp*Ru complexes has also been tested, and the substitution did not show noticeable differences in the reactivity described in this paper.

Synthesis and Characterization of η^1 -Alkynone Complexes. The treatment of fluorobenzene solutions of complexes 1 and 2 with alkynyl ketones, PhC \equiv CCOR (R = Ph, Me), in the presence of NaBAR₄^F produces a slow color change from the initial light yellow to darker colors ranging from green to violet. The reaction is complete in 30 min at 0 °C for the 4-phenyl-3-butyne-2-one derivatives, whereas the slower reaction with diphenylpropynone requires stirring the mixture for 2 h at room temperature. The reaction products are metastable with regard to isomerization

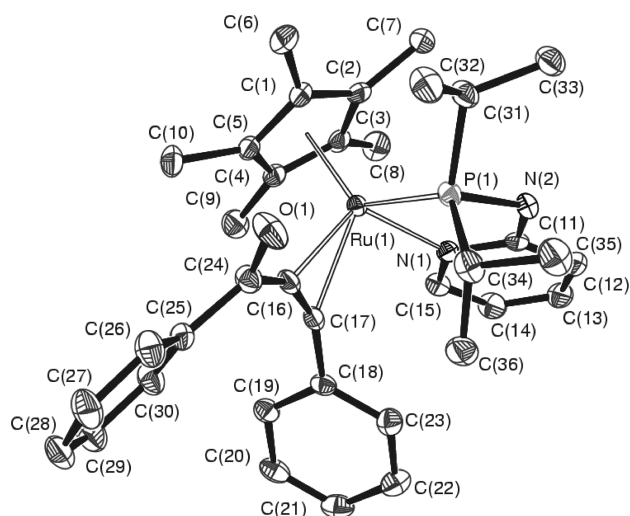


Figure 1. ORTEP view of the cation of [Cp*Ru(η^2 -PhC \equiv CCOPh)($\kappa^2\text{P},\text{N}^1\text{Pr}_2\text{PNHPy}$)] [BPh₄] (12). Selected bond lengths (Å) and angles (deg): Ru1–C16 = 2.125(3), Ru1–C17 = 2.178(2), Ru1–P1 = 2.3057(9), Ru1–N1 = 2.121(2), C16–C17 = 1.260(4), C16–C24 = 1.460(4), C17–C18 = 1.461(4); C16–Ru1–C17 = 34.01(10), C16–C17–C18 = 152.8(3), C17–C16–C24 = 150.3(3), P1–Ru1–N1 = 79.62(6).

to vinylidene (particularly those derived from the 4-phenyl-3-butyne-2-one activation) and very labile when treated with acetone, yielding the corresponding acetone adducts. In absence of better ligands, these compounds are isolable as dark solids (brown to violet), which should be stored at low temperature to prevent isomerization to vinylidene even in the solid state.

The IR and NMR spectra, elemental analysis, and the aforementioned reactivity support the presence of the η^1 -O-ketone adducts (Scheme 1) [TpRu(η^1 -O=C(R)C \equiv CPh)($\kappa^2\text{P},\text{N}^1\text{Pr}_2\text{PXPY}$)] [BAR₄^F] ($\text{X} = \text{CH}_2$, R = Me (5), Ph (6); $\text{X} = \text{S}$, R = Me (7), Ph (8)).

Most of the spectroscopic features (IR and NMR) of complexes 5–8 are comparable to those of the free organic species (Table 1), which are in good agreement with the existence of a weak metal–ligand interaction, and thus the electronic distribution along the ligand remains almost unchanged. The sharp and intense IR $\nu(\text{C}\equiv\text{C})$ absorptions in the range 2159–2204 cm^{-1} clearly rule out the presence of π -alkyne species, the bands for which are typically found between 1700 and 2000 cm^{-1} . The $^{13}\text{C}\{^1\text{H}\}$ NMR spectra show two signals at around 86 and 107 ppm for the quaternary alkynyl carbon atoms. Whereas the first signal is only slightly shifted 1–2 ppm upfield compared to that for the free alkynyl ketone, the second signal is somewhat more affected by the coordination to the metal (12–17 ppm downfield). In all cases, no C–P coupling is observed, and the $^{13}\text{C}\{^1\text{H}\}$ CO chemical shift (δ 189–190 ppm) is in the normal range for organic carbonyl groups. These data also rule out the possibility of a η^2 -ketone complex, for which the CO signal should clearly be shifted upfield.²⁰ Therefore, it seems reasonable to propose the presence of a σ -bonded alkynyl ketone ligand coordinated through the oxygen atom in compounds 5–8. Recently, Shaw et al. have reported the formation of σ -keto alkynyl complexes with the [CpRu(PPh₃)₂]⁺ fragment.¹³

Synthesis and Characterization of π -Alkyne Complexes. The treatment of the Cp*Ru complexes 3 and 4 with the alkynyl ketones PhC \equiv CCOR (R = Ph, Me), in methanol at room temperature and in the presence of NaBPh₄, causes the immediate

Table 3. Selected Bond Lengths and Angles for **12** and Related Ru–Alkyne Complexes

compd	Ru–C (Å)	C–C (Å)	bent-back angle (deg)
[Cp*Ru(ⁱ Pr ₂ PNHPy)(η^2 -PhC≡COPh)] ⁺ (12)	2.125	1.260	27.2
	2.178		29.7
[Cp*Ru(PEt ₃) ₂ (η^2 -HC≡CH)] ⁺ ⁵	2.182	1.220	
	2.180		
[CpRu(PMe ₂ Ph) ₂ (η^2 -HC≡CH)] ⁺ ²⁵	2.204	1.224	
	2.209		
[Cp*Ru(η^6 -diene)] ⁺ ²⁶	2.222	1.237	
	2.326		
[Cp*Ru(η^3 -allyl)(η^2 -PhC≡CPh)] ²⁷	2.135	1.261	29.3
	2.133		29.2
[(η^5 -C ₂ B ₉ H ₁₁)Ru(CO) ₂ (η^2 -MeC≡CPh)] ²⁸	2.302	1.228	23.4
	2.308		18.4
[(Tripod)Ru(η^2 -PhC≡CPh)] ⁺ ^{a,29}	2.183	1.272	31.9
	2.211		32.2
[Ru(P ₃ O ₉)(MeC≡CCO ₂ Et)(dppf)][PPN] ^{b,14}	2.203	1.169	19.45
	2.130		49.23
[CpRu(dppf)(η^2 -EtC≡CMe)] ⁺ ¹⁵	2.232	1.228	35.94
	2.202		26.42

^a Tripod = η^5 : η^1 : η^1 -MeC(CH₂Cp)(CH₂PPh₂)₂. ^b PPN = (Ph₃P)₂N⁺.

precipitation of yellow solids, isolated and characterized as the π -alkyne complexes (Scheme 2) [Cp*Ru(η^2 -PhC≡CCOR)-(κ^2 P,N-ⁱPr₂PXPY)][BPh₄] (X = CH₂, R = Me (**9**), Ph (**10**); X = NH, R = Me (**11**), Ph (**12**)). These compounds are not labile against weak nucleophiles such as acetone, and they do not isomerize to vinylidene even at high temperatures and long reaction times. Compounds **9**–**12** were heated at 80 °C for 5 days without noticeable changes. The use of higher temperatures (DMF, 140 °C, 24 h) leads to a mixture of decomposition products, including the two-step release of the pyridylphosphine and the formation of the sandwich complex [Cp*Ru(η^6 -C₆H₅BPh₃)].²¹ The [B(Ar^F)₄] analogue of compound **11** has also been heated at 120 °C in 1,1,2,2-tetrachloroethane-*d*₂ and the process monitored by ³¹P{¹H} NMR. None of the detected species correspond to vinylidene, as shown in the ¹³C{¹H} NMR spectrum by the lack of the characteristic low-field resonance. Instead, processes involving alkyne rotation, alkyne release, and the aforementioned decomposition pathways are detected.

The IR spectra show very broad absorptions centered at 1828, 1800, 1842, and 1871 cm⁻¹, respectively, for complexes **9**–**12** (Table 2). Although the elemental analyses match well with a pure substance of the expected empirical formula, the NMR spectra display two sets of signals. The ratio of the major to minor product is >78% based on the ³¹P{¹H} signal. This observation is attributed to the existence of two alkyne rotamers due to the restricted rotation about the Ru–alkyne bond.²² The ¹³C{¹H} NMR of the major product shows doublet signals for the alkyne quaternary carbon atoms (Table 2).

All these features are quite characteristic of the presence of a η^2 -alkyne ligand, and this has been definitively confirmed by X-ray diffraction analysis of suitable monocrystals of **12**, obtained by slow diffusion of Et₂O into an acetone solution of the complex. An ORTEP view of the cation complex **12** is shown in Figure 1 with selected bond lengths and angles.

The geometry around the ruthenium atom in **12** can be described as a three-legged piano stool, with the cyclopentadienyl ligand occupying three sites, the alkyne midpoint considered

as one site, and the pyridylphosphine occupying the other two coordination positions. The alkyne is asymmetrically bonded to ruthenium (2.125(3), 2.178(2) Å), which is consistent with the presence of an asymmetric ruthenium center and two different substituents on the alkyne. The alkyne carbon atom bearing the phenyl group is farther from ruthenium than that bonded to the acyl group. Although the NMR spectra show the presence of two alkyne rotamers (86:14 ratio for **12**), the crystal structure only corresponds to one of them, likely the major rotamer, with the acyl group in a cisoid disposition to the phosphorus atom and transoid to the pyridyl nitrogen atom. This orientation seems to minimize the steric hindrance by pointing the CO group toward the phosphine isopropyl groups.

The strength of the metal–alkyne interaction can be readily assessed by the metal–C(alkyne) bond distance and the degree to which the substituents on the alkyne ligand are bent back from the C–C axis. Table 3 gives a list of these bond lengths and angles for various π -alkyne complexes related to **12**. The Ru–C16/C17 distances (2.152 Å in average) are at the lower end of the range. Consistent with the alkyne acting as only a two-electron donor, the C16–C17 distance is lengthened to 1.260(4) Å, which is comparable to the mean value (1.269 Å) found in alkyne–metal complexes,²³ and considerably longer than the mean C≡C bond distance for organic disubstituted alkynes (1.192 Å).²⁴ The alkyne substituents are bent back (C16–C17–C18 = 152.8(3)°, C17–C16–C24 = 150.3(3)°), with a deviation from linearity of 27.2 and 29.7°, respectively, confirming a significant π back-bonding interaction from the metal to the alkyne.

It is interesting to compare the structure of complex **12** (which does not isomerize to vinylidene) with the two structurally characterized π -alkyne complexes reported by Ishii et al. (last two entries in Table 3), which do isomerize to vinylidene. In both cases, the ruthenium–alkyne interaction seems slightly weaker than in **12**, exhibiting longer Ru–C distances and shorter C–C bond lengths. However, the bent-back angle is larger at one side of the alkyne in Ishii's complexes (i.e., the COOEt bent-back angle is 49.23°, whereas that for the Me group is 19.45°).

Scheme 3. Synthesis of TpRu–Vinylidene Complexes

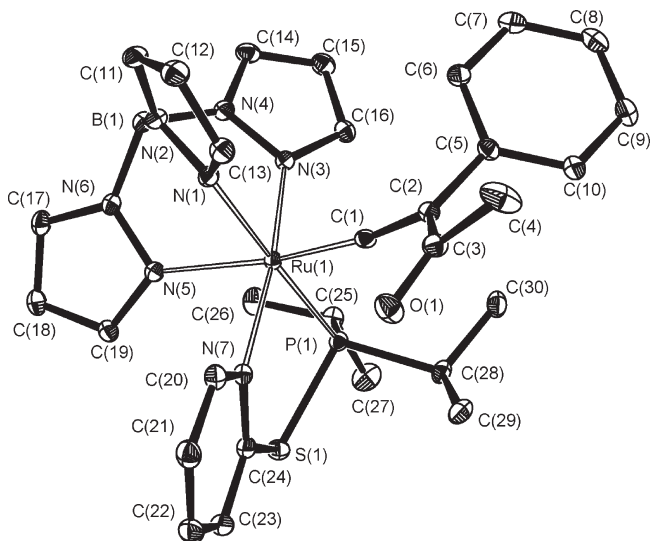
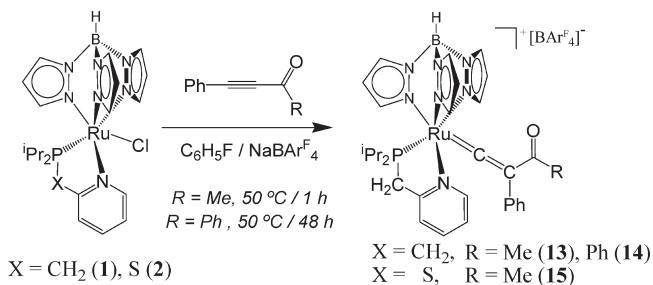


Figure 2. ORTEP view of the cation of $[\text{TpRu}\{\text{=C=C}(\text{COMe})\text{Ph}\}-(\kappa^2\text{P},\text{N}-\text{P}^1\text{Pr}_2\text{SPy})][\text{BARF}_4^+]$ (**15**). Selected bond lengths (Å) and angles (deg): $\text{Ru1}-\text{C1} = 1.805(2)$, $\text{C1}-\text{C2} = 1.329(3)$, $\text{C2}-\text{C3} = 1.489(3)$, $\text{C2}-\text{C5} = 1.496(3)$, $\text{Ru1}-\text{P1} = 2.2916(7)$, $\text{Ru1}-\text{N7} = 2.1326(17)$; $\text{Ru1}-\text{C1}-\text{C2} = 169.94(17)$, $\text{C1}-\text{C2}-\text{C3} = 117.60(18)$, $\text{C1}-\text{C2}-\text{C5} = 118.60(18)$, $\text{P1}-\text{Ru1}-\text{N7} = 83.93(5)$.

Synthesis and Characterization of Disubstituted Keto Vinylidene Complexes. The activation of alkynes by Cp^*Ru and TpRu complexes have yielded substantially distinct compounds, namely the π -alkyne complexes **9–12** and the $\eta^1\text{-O}$ -keto alkyne complexes **5–8**, easily identifiable by their characteristic spectroscopic features. They are also remarkably different in stability: whereas the π -alkyne compounds are stable under an inert atmosphere, the alkynyl ketone adducts undergo spontaneous isomerization to vinylidene both in solution and in the solid state. It is noteworthy that π -alkyne complexes are generally described as reasonable intermediates in the first step of the alkyne–vinylidene isomerization, which has been shown to be the case in the isomerization of terminal alkynes.^{1–6,30}

Therefore, the synthesis of disubstituted vinylidenes can be accomplished either by heating a 1,2-dichloroethane solution of complexes **5–7** or directly from the starting complexes **1** and **2** in fluorobenzene with heating (Scheme 3). As previously observed, the isomerization rate reveals a strong dependence on the ketone substituent ($\text{Me} \gg \text{Ph}$), and thus the preparation of the vinylidene complexes $[\text{TpRu}\{\text{=C=C}(\text{COR})\text{Ph}\}(\kappa^2\text{P},\text{N}-\text{P}^1\text{Pr}_2\text{PXPy})][\text{BARF}_4^+]$ ($X = \text{CH}_2$, $R = \text{Me}$ (**13**), Ph (**14**); $X = \text{S}$, $R = \text{Me}$ (**15**)) requires heating for 1 h at 50 °C in the case of the methyl

Table 4. Selected $^{31}\text{P}\{^1\text{H}\}$ and $^{13}\text{C}\{^1\text{H}\}$ NMR Data (δ) for Compounds **13–18**

compd	$^{13}\text{C}\{^1\text{H}\}$		$^{31}\text{P}\{^1\text{H}\}$
	$\text{Ru}=\text{C}=\text{C}$	$^2J_{\text{CP}}$ (Hz)	
13	357.3	18.2	64.3
14	356.5	19.5	63.6
15	363.1	18.3	123.6
16	357.5	18.8	64.7
17	361.3	18.5	65.7
18	364.8	18.7	65.9

derivatives (**13** and **15**) and for 48 h at 50 °C in the case of the phenyl derivative **14**, in order to complete the reaction. The complex with $X = \text{S}$ and $R = \text{Ph}$ undergoes decomposition during the long reaction time or on heating at higher temperatures. Although the vinylidene complex can be detected, it could not be isolated and characterized properly.

Compounds **13–15** have been characterized by spectroscopy and by the X-ray diffraction analysis of monocrystals of **15** ($X = \text{S}$, $R = \text{Me}$), grown by slow diffusion of petroleum ether into a diethyl ether solution of the complex. Figure 2 gives an ORTEP view of the cationic complex with selected bond lengths and angles.

The X-ray structure of complex **15** shows a distorted-octahedral coordination around the ruthenium center, with three facial coordination sites occupied by the N atoms of the Tp ligand, two other positions by the P and N atoms of the 2-(diisopropylphosphinothio)pyridine ligand, and the sixth position by a linear carbon chain. This ligand exhibits a short Ru–C1 distance of 1.805(2) Å, which reflects the strong back-bonding from the metal characteristic of the vinylidene ligands. The C1–C2 bond length of 1.329(3) Å, and the C1–C2–C3/C1–C2–C5 bond angles (117.60(18) and 118.60(18)°, respectively) fit well with a vinylidene ligand with sp^2 hybridization at C2. The carbon chain is almost linearly assembled to ruthenium ($\text{Ru1}-\text{C1}-\text{C2} = 169.94(17)^\circ$). These data compare well with the structural information available for related complexes such as $[\text{CpRu}\{\text{=C}=\text{C}(\text{COPh})\text{Ph}\}(\text{PPh}_3)_2][\text{BARF}_4^+]$ (1.818 and 1.335 Å; 120.06, 119.74, and 170.73°),¹³ $[\text{CpRu}\{\text{=C}=\text{C}(\text{Ph})(p\text{-C}_6\text{H}_4\text{OMe})\}(\text{dppe})][\text{BARF}_4^+]$ (1.838 and 1.327 Å; 122.5, 118.4, and 173.3°),¹⁵ and $[\text{TpRu}\{\text{=C}=\text{C}(\text{COPh})\text{Ph}\}(\text{P}^i\text{Pr}_2\text{Me})(\text{MeCN})][\text{BARF}_4^+]$ (1.814 and 1.322 Å; 118.7, 124.1, and 177.7°).¹⁸ The enone moiety ($\text{C}=\text{CCOMe}$) is almost planar (dihedral angles: $\text{C1}-\text{C2}-\text{C3}-\text{C4} = 13.15^\circ$, $\text{C1}-\text{C2}-\text{C3}-\text{O1} = 12.17^\circ$), adopting an *s-cis* conformation with the CO group pointing to the pyridine side.

In addition to the X-ray data, the most characteristic vinylidene feature can be found in the $^{13}\text{C}\{^1\text{H}\}$ NMR spectra. The presence of a carbene carbon atom is revealed by characteristic low-field resonances observed at 357.3, 356.5, and 363.1 ppm, respectively, for compounds **13–15**, which appear as doublets with C–P coupling constants of 18–19 Hz. A summary of the main spectroscopic features of all the vinylidene complexes reported in this paper is shown in Table 4.

Activation of Internal Alkynes Not Bearing a Ketone Group. In order to test the synthesis of vinylidene complexes from internal alkynes not bearing a ketone group, we have tried the reaction of the starting complex **1** with a series of disubstituted alkynes $\text{RC}\equiv\text{CR}'$ (R, R' : Ph, COOMe; Me, COOEt; Ph, Ph).

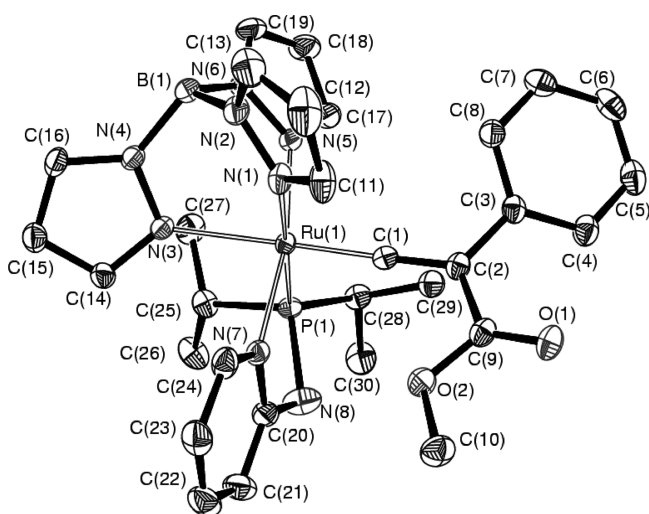
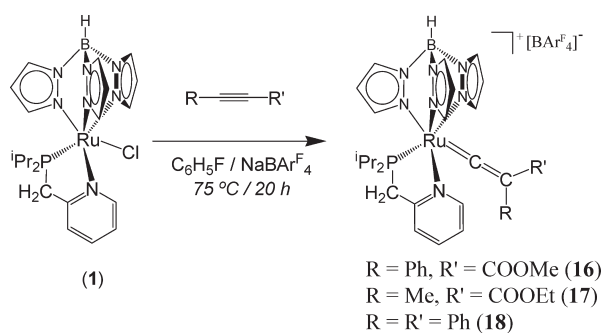
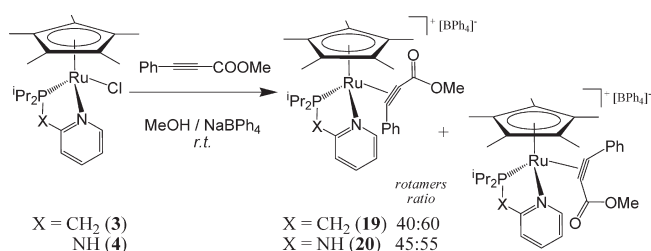
Scheme 4. Synthesis of TpRu–Vinylidene Complexes without a Ketone Group


Figure 3. ORTEP view of the cation of $[\text{TpRu}\{\text{=C=C}(\text{COOMe})\text{-Ph}\}(\kappa^2\text{P,N-P}^2\text{Pr}_2\text{CH}_2\text{Py})][\text{BARF}_4]$ (**16**). Selected bond lengths (Å) and angles (deg): Ru1–C1 = 1.803(2), C1–C2 = 1.330(3), C2–C3 = 1.490(4), C2–C9 = 1.480(3), Ru1–P1 = 2.3086(8), Ru1–N7 = 2.105(2); Ru1–C1–C2 = 171.1(2), C1–C2–C3 = 119.1(2), C1–C2–C9 = 119.7(2), P1–Ru1–N7 = 81.95(6).

The corresponding vinylidenes $[\text{TpRu}(\text{=C=CRR}')(\kappa^2\text{P,N-P}^2\text{Pr}_2\text{CH}_2\text{Py})][\text{BARF}_4]$ (R, R': Ph, COOMe (**16**); Me, COOEt (**17**); Ph, Ph (**18**)) have been isolated as orange-brown solids after heating the reaction mixture for at least 20 h at 75 °C (Scheme 4).

Attempts to isolate any intermediate failed and yielded only a complex mixture of decomposition products. However, the direct preparation from **1** gave complexes **16–18** in pure form in moderate to good yields. These complexes have been characterized by spectroscopy (showing the typical carbenic resonance as doublets at 357.5, 361.3, and 364.8 ppm, respectively, in their $^{13}\text{C}\{^1\text{H}\}$ NMR spectra; see Table 4), and particularly by the X-ray structure of complex **16**. An ORTEP view of the cation complex is shown in Figure 3 with selected bond lengths and angles.

The structure of **16** resembles that previously described for complex **15**, showing a distorted-octahedral geometry around the ruthenium center and the presence of the vinylidene ligand with almost identical bond lengths and angles. However, the ligand conformation is s-trans, showing a planar C=CCOOMe

Scheme 5. Synthesis of Cp*Ru– π -Alkyne Complexes without a Ketone Group


group (torsion angles: C1–C2–C9–O1 = 6.49°, C1–C2–C9–O2 = 6.09°).

On the other hand, the activation of the internal alkyne $\text{PhC}\equiv\text{CCOOMe}$ by the starting complexes **3** and **4** yields the expected π -alkyne derivatives $[\text{Cp}^*\text{Ru}(\eta^2\text{-PhC}\equiv\text{CCOOMe})\text{-}(\text{P}^2\text{Pr}_2\text{XPy})][\text{BPh}_4]$ (X = CH₂ (**19**), NH (**20**)), which do not isomerize to vinylidene (Scheme 5). The spectra of complexes **19** and **20** exhibit the same characteristics observed for the related compounds **9–12** (selected NMR and IR data are shown in Table 2), which are consistent with the existence of a π -alkyne ligand: the presence of rotamers (40:60 ratio for **19**, 45:55 ratio for **20**, based on the integrals of the $^{31}\text{P}\{^1\text{H}\}$ NMR spectra), C–P coupling for the alkyne quaternary carbon $^{13}\text{C}\{^1\text{H}\}$ NMR signals, and broad IR absorptions at 1842 and 1856 cm^{-1} , respectively.

These results confirm that Cp^*Ru complexes stabilize the π -alkyne as a final product which is reluctant to isomerize to vinylidene regardless of the substituents on the alkyne. On the other hand, TpRu complexes seem to avoid π -alkyne formation by stabilizing the η^1 -ketone adduct as a metastable intermediate to vinylidene. Despite the formal similarities between Tp and Cp/Cp* ligands, the obvious differences in size and electronic properties result in a different chemistry.³¹ In particular, the steric bulk and the rigidity of the Tp ligand appear to disfavor higher coordination numbers of the metal center, which may favor the η^1 -keto alkyne with regard to the η^2 -alkynyl ketone coordination.

Kinetic Studies of the Alkynone to Vinylidene Isomerization in Solution. A qualitative analysis of the experimental conditions required for the η^1 -keto alkyne to vinylidene isomerization shows that the presence of a ketone group significantly increases the reaction rate (COMe \gg COOMe; see synthesis of compound **13** vs **16**) and that the ketone substituent also plays an important role in the isomerization rate (Me \gg Ph; see synthesis of **13** vs **14**).

Quantitative kinetic measurements have been obtained by monitoring the evolution of the $^{31}\text{P}\{^1\text{H}\}$ NMR signals of compounds **5–7** in 1,1,2,2-tetrachloroethane-*d*₂ solution at variable temperature. In all cases, the isomerization processes obey a first-order rate law. Thus, the first-order rate constants have been obtained at different temperatures and the corresponding Eyring plots provide the activation parameters. $\ln(I_t/I_0)$ vs time and Eyring plots can be found in the Supporting Information. Table 5 gives the rate constants at each temperature, the temperature ranges at which the isomerization rates were measurable, and the Eyring activation parameters. The results of our previous kinetic study on the $[\text{TpRu}(\kappa^2\text{P,N}^2\text{-Pr}_2\text{PNHpy})]^+$ fragment are shown for comparative purposes.¹⁸

In all cases ΔG_{298}^\ddagger is around 23–25 kcal mol^{-1} , with activation enthalpies of 17–22 kcal mol^{-1} and slightly negative

Table 5. Rate Constants and Activation Parameters for the η^1 -Keto Alkyne \rightarrow Vinylidene Isomerization

T, K	$10^{-4}k, \text{s}^{-1}$			
	ligand, alkyne			
	ⁱ Pr ₂ PNHPy, PhC≡CCOMe ¹⁸	ⁱ Pr ₂ PCH ₂ Py, PhC≡CCOMe (5 \rightarrow 13)	ⁱ Pr ₂ PSPy, PhC≡CCOMe (7 \rightarrow 15)	ⁱ Pr ₂ PCH ₂ Py, PhC≡CCOPh (6 \rightarrow 14)
313	2.36(4)	1.80(2)		
318	3.91(5)	4.40(8)		
323	6.16(12)	6.80(9)	2.40(4)	
328	11.1(2)	10.3(2)	3.80(7)	
333	13.1(3)	17.8(5)	5.90(14)	
338	21.1(3)		11.68(23)	
343			14.2(4)	2.47(6)
348				3.97(9)
353				5.10(12)
358				8.22(19)
363				12.5(4)

	ligand, alkyne			
	ⁱ Pr ₂ PNHPy, PhC≡CCOMe ¹⁸	ⁱ Pr ₂ PCH ₂ Py, PhC≡CCOMe (5 \rightarrow 13)	ⁱ Pr ₂ PSPy, PhC≡CCOMe (7 \rightarrow 15)	ⁱ Pr ₂ PCH ₂ Py, PhC≡CCOPh (6 \rightarrow 14)
ΔH^\ddagger , kcal mol ⁻¹	17.6 \pm 1.0	21.9 \pm 1.9	19.9 \pm 1.6	18.9 \pm 1.0
ΔS^\ddagger , cal mol ⁻¹ K ⁻¹	-19 \pm 3	-5 \pm 6	-13 \pm 5	-20 \pm 3
ΔG^\ddagger_{298} , kcal mol ⁻¹	23.2 \pm 1.3	23.5 \pm 2.5	24.0 \pm 2.1	24.9 \pm 1.4

values for the activation entropies of the process. The first-order kinetic data and the activation parameters point to a simple concerted process. The negative activation entropy may be understood as a decrease of translational, rotational, and vibrational degrees of freedom on the route to the transition state, suggesting a concerted 1,2-sigmatropic shift of the alkyne substituent for the rate-determining step of the reaction.

These results are in good agreement with the literature for similar alkyne/vinylidene isomerization processes, such as the concerted 1,2-SiMe₃ shift in *trans*-[RhCl(L)(PPR₃)₂] ($\Delta H^\ddagger = 19.8 \text{ kcal mol}^{-1}$, $\Delta S^\ddagger = -4.8 \text{ cal mol}^{-1} \text{ K}^{-1}$).^{8c} Kinetic studies on terminal alkyne isomerization via a direct 1,2-H shift have been reported with comparable activation parameters.³² However, these are the first complete kinetic studies about the migration of carbon functional groups in metal-mediated alkyne/vinylidene isomerization. The migration of acetyl, formyl, or carbomethoxy groups in pure organic systems, such as the migration of an acetyl group in 1,3-cyclohexadiene ($\Delta S^\ddagger = -7.8 \text{ cal mol}^{-1} \text{ K}^{-1}$), usually requires higher activation energies and similar negative values of ΔS^\ddagger .³³

The rate constants and the temperature range at which they have been measured clearly indicate that the effect of the spacer group X in the pyridylphosphine ligand (PⁱPr₂XPy) is very small. The process is only slightly faster with X = NH, CH₂ than with X = S as linking group. The effect of the ketone group (COR) is much stronger, where the derivatives with R = Ph isomerize too slowly to be measured, except for the 6 \rightarrow 14 isomerization (X = CH₂, R = Ph). This process requires temperatures 30 K higher than that for the isomerization of 5 (X = CH₂, R = Me), and 20 K higher than that for 7 (X = S, R = Me) to reach similar reaction rates. The large effect of the R group (PhC≡CCOR, R = Me, Ph) on the reaction rate shows that the migrating group is predominantly the acyl group.

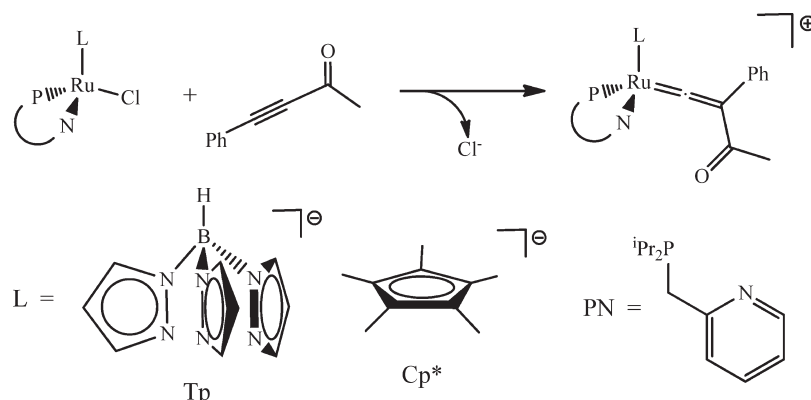
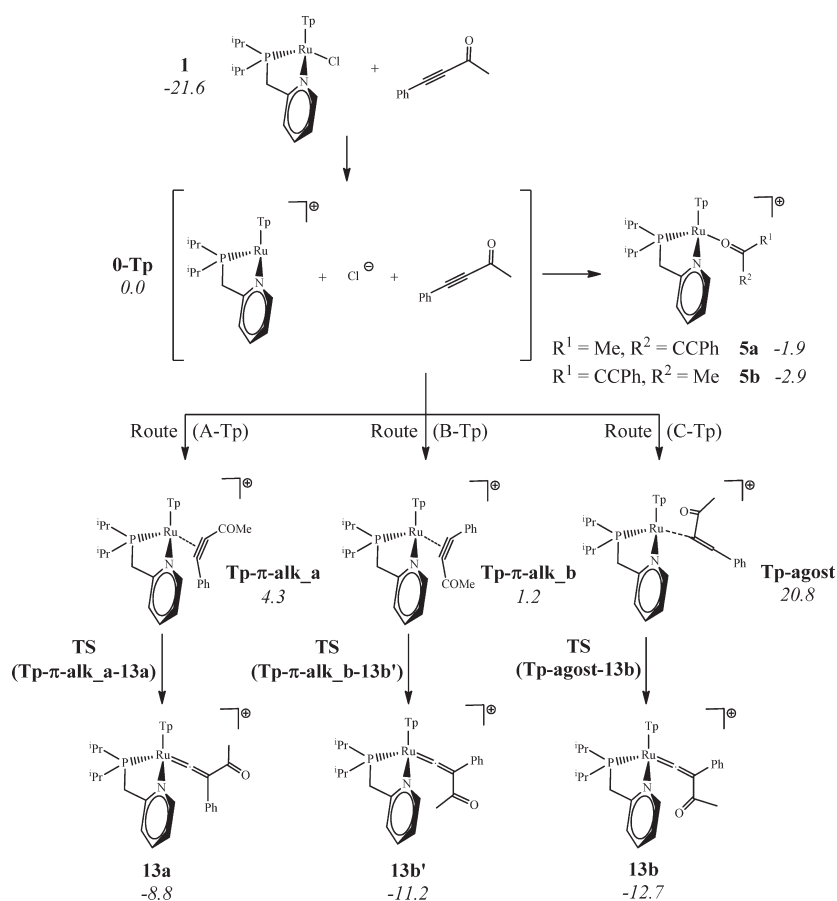
The ³¹P{¹H} NMR monitoring of the reaction during the kinetic studies did not show any signals other than those corresponding to

the η^1 -keto alkyne and the final vinylidene complexes. In addition to the fact that π -alkynes in the described Cp^{*}Ru systems do not rearrange to vinylidene, this opens two questions: what is the role of π -alkyne species in the isomerization process, and how can these two related ruthenium complexes, differing only in the presence of a Tp or a Cp^{*} ligand, exhibit such a contrasting behavior regarding the isomerization of the same internal alkyne to vinylidene?

For the first question, it is noteworthy that Gladysz et al. have reported that C=O/ σ type bonds are kinetically favored with respect to C=C and C≡C/ π bonds, which are the thermodynamically preferred binding sites for the coordination of α , β -unsaturated aldehydes and ketones to the rhenium fragment [CpRe(NO)(PPh₃)]⁺.³⁴ On the basis of our experimental results and the previous literature, a mechanistic proposal was already outlined in our last publication on this subject. However, to the best of our knowledge, there is no precedent of a thorough theoretical study on the mechanistic features of the isomerization of internal alkynes, which can eventually justify the contradictory results obtained for Tp and Cp^{*} ruthenium complexes.

Kinetic Studies of the Alkynone to Vinylidene Isomerization in the Solid State. An additional support for a concerted mechanism is the existence of solid-state isomerization, which was described in detail in our last paper.¹⁸ In this paper, we have also followed the solid-state isomerization 5 \rightarrow 13 by IR spectroscopy. The starting η^1 -ketone complex displays a strong $\nu(\text{C}\equiv\text{C})$ vibration at 2204 cm⁻¹ (with a shoulder at 2160 cm⁻¹ characteristic of the 4-phenylbutyn-2-one derivatives). During the isomerization to vinylidene, the $\nu(\text{C}\equiv\text{C})$ IR band gradually disappears. Monitoring the integrated intensity of the $\nu(\text{C}\equiv\text{C})$ IR band as a function of time has allowed us to evaluate the advance of isomerization at different temperatures (37, 45, and 50 °C).

Scheme 6. Ligands and Substrate Used in the Calculations

Scheme 7. Alkynone–Vinylidene Isomerization for Tp Complex **1**^a

^aRelative ΔG_{FBZ} values are given in kcal mol⁻¹ with respect to the separated species.

The corresponding α (fraction of transformed solid) vs time curves $\ln(I_t/I_0)$ for the **5** \rightarrow **13** isomerization in the solid state at 37, 45, and 50 °C can be found in the Supporting Information, as well as the graphics corresponding to a fit to the Avrami–Erofeev equation.³⁵ In contrast to the reaction in solution, the solid-state isomerization does not fit with a first-order rate law, as the process considerably slows down at values of α around 0.5–0.6, requiring 3–4 days for completion. The n values measured at 37,

45, and 50 °C were 0.91(9), 0.51(4), and 0.59(7), respectively. The mechanism controlling the reaction should be nucleation and nuclei growth, rather than the chemical reaction itself. Values of the Avrami exponent around 0.5 correspond to the thickening of large plates after lateral collision.³⁶ Thus, at a certain value of α (around $\alpha = 0.5$ for us), the product crystal nuclei get into contact with each other, the overlapping of the product nuclei takes place, and a decrease of the reaction rate is observed.

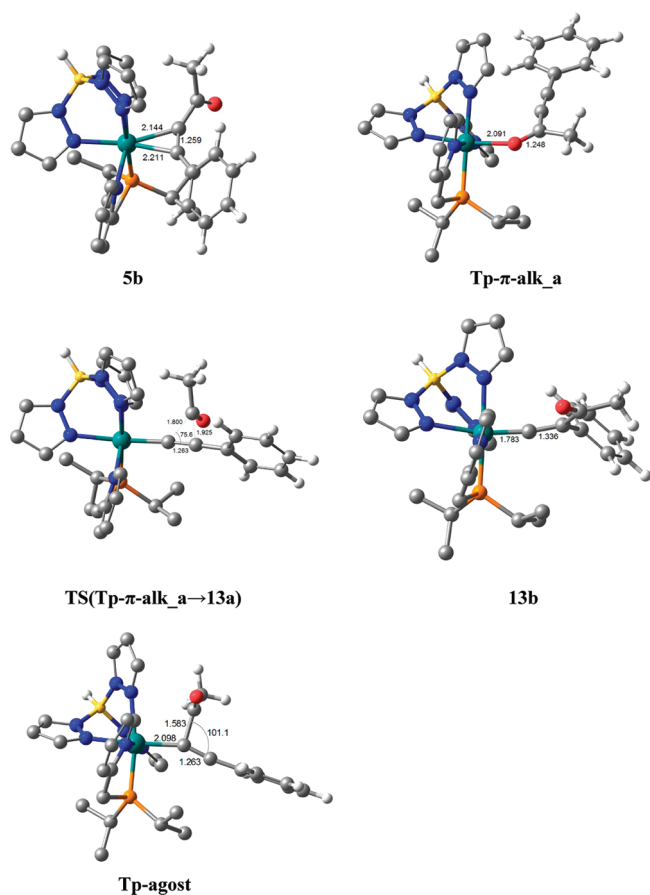


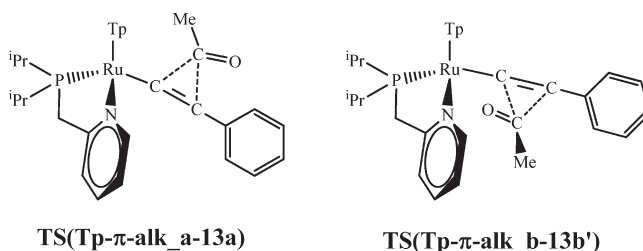
Figure 4. Optimized structures of selected species of the alkyne–vinylidene isomerization in the TpRu complex. Bond distances are given in Å and angles in deg. Hydrogen atoms on Tp and P,N ligands have been removed for clarity.

Computational Study of the Alkyne to Vinylidene Isomerization. In order to analyze the mechanism of the π -alkyne \rightarrow vinylidene isomerization of internal alkynes and to explain the contrasting results obtained for Tp and Cp* ruthenium complexes, we have undertaken a theoretical study of the formation of disubstituted vinylidenes from the internal alkyne PhC \equiv CCOMe (**A-alk**) on the coordination sphere of ruthenium complexes [LRu(κ^2P,N -Pr₂PCH₂Py)Cl] (L = Tp, Cp*). No model has been used in the computational study, calculations being performed using the actual experimental complexes **1** and **3** including solvent effects with a continuum description of the solvent (fluorobenzene in the case of Tp complexes and methanol in the case of Cp* complexes). All the values collected in the energy profiles are relative Gibbs energies in solution (ΔG_{soln}). Scheme 6 summarizes the systems used in the calculations.

Isomerization in the TpRu Complex. The isomerization has been studied in fluorobenzene (FBZ), the solvent used in the experiments. Scheme 7 shows all the calculated species and their relative Gibbs energies, taking as zero energy the separated [TpRu(κ^2P,N -PⁱPr₂CH₂Py)]⁺ (**0-Tp**), Cl[−], and PhC \equiv CCOMe (**A-alk**). The optimized structures of selected Tp species relevant for the alkyne–vinylidene isomerization are shown in Figure 4.

The chloride precursor [TpRuCl(κ^2P,N -PⁱPr₂CH₂Py)] (**1**) is much more stable than the separated species, indicating the difficulty of releasing the halide. Indeed, the chloride abstraction

Scheme 8. Transition States of the 1,2-Acyl Shift in the Tp Complexes



for the TpRu starting complexes is only possible in the presence of NaBAR^F₄. The relative stabilities of the η^1 -O-ketone and π -alkyne adducts also agree with the experimental evidence. Calculations show that the η^1 -ketone species **5** are favored compared to the π -alkyne intermediates **Tp- π -alk**; indeed, the latter have Gibbs energies above those of the separated species **0-Tp** (4.3 kcal mol^{−1} for **Tp- π -alk_a** and 1.2 kcal mol^{−1} for **Tp- π -alk_b**) and, therefore, they should be hardly detected. The calculated $\nu(\text{C}\equiv\text{C})$ absorptions for the two conformational isomers of **5** (**5a**, 2201 cm^{−1}; **5b**, 2180 cm^{−1}) are in good agreement with the experimental IR $\nu(\text{C}\equiv\text{C})$ absorptions of complex **5** (2159–2204 cm^{−1}).³⁷

Despite the η^1 -O-keto alkyne being the most stable adduct resulting from the initial interaction of **0-Tp** and the alkyne, it is reasonable to assume that a π -alkyne intermediate is required in order to make the isomerization proceed. The existence of a weak metal–ligand interaction in **5** (ΔG_{FBZ} values of binding of only 1.9 kcal mol^{−1} in **5a** and 2.9 kcal mol^{−1} in **5b**) makes such intermediates accessible by a dissociation–association process. In this way the nondetected π -alkyne rotamers **Tp- π -alk_a** and **Tp- π -alk_b** can be formed.³⁸ From these intermediates a 1,2-acyl migration leads to the vinylidene isomers **13a,b** after crossing transition states TS(**Tp- π -alk_a**→**13a**) and TS(**Tp- π -alk_b**→**13b**) depicted in Scheme 8 and placed 20.8 and 26.1 kcal mol^{−1} above the separated reactants, respectively (routes A-Tp and B-Tp, Scheme 7). Vinylidene complexes are much more stable than the alkynes, giving the thermodynamic driving force for the isomerization.

Structural and electronic changes along the 1,2-acyl migration in the Tp complex are collected in Table 6. In comparison with the migration in the metal-free system, the transition states in the TpRu complex show more synchronous C–C bond-making and bond-breaking processes, the C(O)–C_α distance being only slightly shorter than the C(O)–C_β distance. The C_α–C_β bond distances of transition states are practically the same as in related π -alkyne geometries.

The electrophilic nature of the 1,2-shift is also evident from the charges shown in Table 6: the acyl migrates with a substantial amount of positive charge. The presence of the metal allows a better distribution of the negative charge created in C_β.

Starting from the most stable η^1 -O-ketone rotamer **5b**, the overall activation barriers are 23.7 and 29.0 kcal mol^{−1} for routes A-Tp and B-Tp, respectively. The Gibbs activation energy of the A-Tp pathway is very close to the experimentally determined ΔG_{298}^\ddagger for the **5** \rightarrow **13** isomerization (23.5 \pm 2.5 kcal mol^{−1}, Table 5), stressing the reliability of the proposed mechanism.

Pathway A-Tp leads directly to the vinylidene rotamer **13a**, in which the carbonyl group of the acyl substituent is placed *s-trans* with respect to the C=C bond of the vinylidene moiety and anti

Table 6. Structural and Electronic Changes along the 1,2-Acyl Migration in Complex 1

	Tp- π -alk_a	TS(Tp- π -alk_a \rightarrow 13a)	Tp- π -alk_b	TS(Tp- π -alk_a \rightarrow 13b')
$d(\text{C}(\text{O})-\text{C}_\alpha)$, Å	1.475	1.800	1.463	1.788
$d(\text{C}(\text{O})-\text{C}_\beta)$, Å	2.634	1.925	2.606	1.904
$d(\text{C}_\alpha-\text{C}_\beta)$, Å	1.259	1.263	1.269	1.263
$q(\text{COMe})$	+0.07	+0.24	+0.00	+0.20
$q(\text{C}_\alpha)$	-0.06	+0.01	-0.11	+0.02
$q(\text{C}_\beta)$	+0.05	-0.00	+0.12	-0.01

Table 7. NBO Analysis of Intermediate Tp-agost

NBO label	localized orbital	occ	energy, au	E_{deloc}^a
BD(1)	$\sigma(\text{C}(\text{O})-\text{C}_\alpha)$	1.779	-0.685 52	^b
LP*(1)	$n^*(\text{C}_\beta)$	0.683	-0.189 25	35.4
BD*(1)	$\sigma^*(\text{Ru}-\text{C}_\alpha)$	0.320	+0.129 57	7.6
LP*(4)	$n^*(\text{Ru})$	0.438	+0.733 07	5.0
LP*(5)	$n^*(\text{Ru})$	0.208	+0.216 34	2.6
LP*(6)	$n^*(\text{Ru})$	0.191	+0.238 35	4.4

^a E_{deloc} in kcal mol⁻¹. ^b E_{deloc} values are given with respect to the $\sigma(\text{C}(\text{O})-\text{C}_\alpha)$ orbital.

with respect to the pyridine ligand. This is not the most stable rotamer of vinylidene. The most stable orientation of the coordinated vinylidene is found in **13b** (C=O *s-cis* with respect to the C=C bond and *syn* with respect to the pyridine), which also corresponds to the arrangement found in the X-ray structure of **15** (Figure 2). By means of selected rotation processes, **13a** can easily evolve to **13b**. We have calculated the rotational barriers for the pathway connecting **13a** with **13b**, showing an overall barrier of 8.5 kcal mol⁻¹, which is considerably lower than the Gibbs energy of activation for the 1,2-acyl shift.

For the alkyne–vinylidene transformation of terminal alkynes on ruthenium half-sandwich complexes, in addition to the direct 1,2-hydrogen shift, it has been proposed that the process can go through a preliminary slippage to an η^2 -(C–H) agostic intermediate which then undergoes the 1,2-hydrogen shift.^{30b,39} For the isomerization of an internal alkyne the equivalent agostic intermediate should be a η^2 -(C–C) agostic species. Agostic C–C structures have been described,⁴⁰ including with acyl ligands.^{40a} We have been able to find such a structure (Tp-agost, Figure 4).⁴¹ The intermediate Tp-agost lies 20.8 kcal mol⁻¹ above **0-Tp** and 19.6 kcal mol⁻¹ above the most stable π -alkyne rotamer (Tp- π -alk b). The structural features of Tp-agost place it at an advanced stage of the acyl shift: the C(O)–C α bond distance is elongated to 1.583 Å, i.e., it is 0.167, 0.120, and 0.138 Å larger than in η^1 -ketone **8b**, π -alkyne **8b**, and free alkyne **A-alk**, respectively, and in addition the C(O)–C α –C β angle has closed to 101°. To ascertain whether this structure is an artifact of the calculation, we have reoptimized it using another functional (M06). Indeed, it remains as a minimum with similar geometrical parameters (C(O)–C α bond distance of 1.578 Å and C(O)–C α –C β angle of 101.2°) and relative Gibbs energy (17.7 kcal mol⁻¹ above Tp- π -alk b). From this intermediate the isomerization process (route C-Tp) easily evolves through TS(Tp-agost \rightarrow 13b), yielding directly the most stable vinylidene rotamer **13b**. This process has an overall activation barrier (from **5b** to TS(Tp-agost \rightarrow 13b)) of 25.6 kcal mol⁻¹. This barrier is only 1.9 kcal mol⁻¹ higher than that of route A-Tp involving the π -alkyne intermediate and cannot be discarded as a feasible pathway.

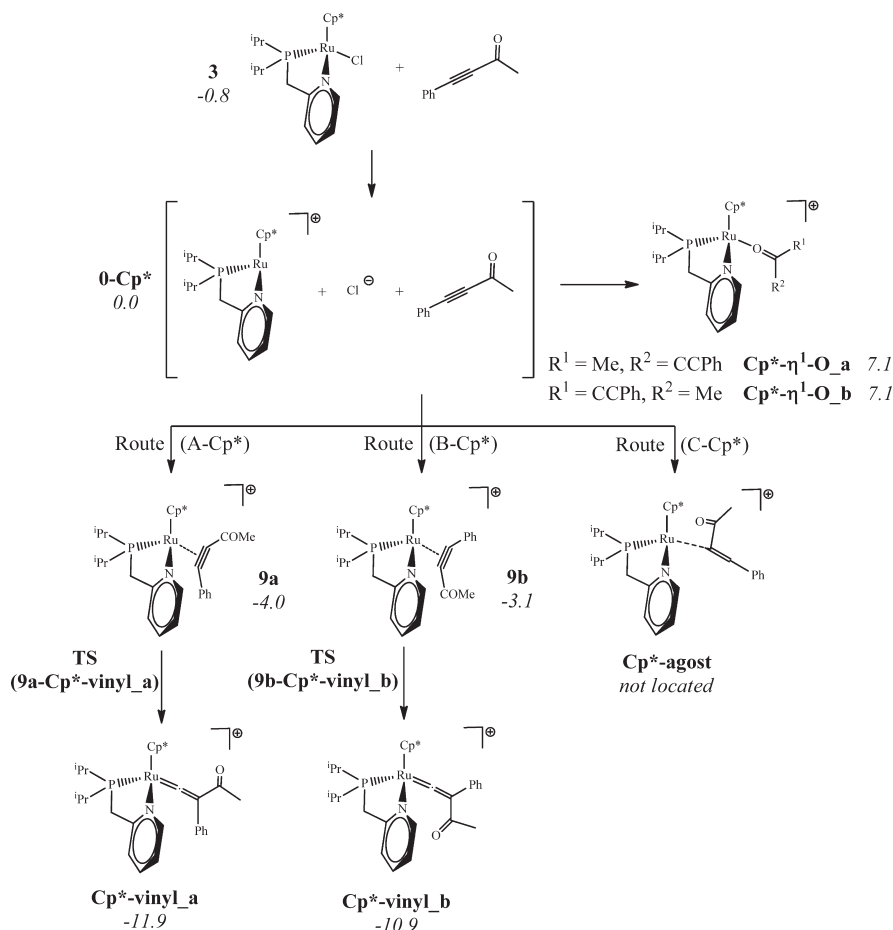
We have analyzed the electronic structure of intermediate Tp-agost with the NBO method (Table 7). The $\sigma(\text{C}(\text{O})-\text{C}_\alpha)$ orbital exhibits low occupancy, and the $\sigma(\text{C}(\text{O})-\text{C}_\alpha)$ to $n^*(\text{C}_\beta)$ delocalization energy is quite significant: 35.4 kcal mol⁻¹. Electron delocalization from this orbital to metal empty orbitals is also important (entries 3–6 in Table 7).

To assess the role that agostic C–C intermediates could play in the isomerization of internal alkynes and to test the stability of this particular structure, we have performed optimizations changing the acyl group COMe to H, Me, and Ph groups (PhC \equiv CR alkynes, R = H, Me, Ph). When the group is H (terminal alkyne), the structure evolves to the well-known η^2 -(C–H) agostic interaction. The optimization containing a Me group leads to the π -alkyne structure, and that containing Ph group yields the vinylidene species. It is not possible to find such η^2 -(C–C) agostic intermediates when the phenyl group is replaced by a methyl (MeC \equiv CCOMe alkyne). This observation points out that electron delocalization toward the phenyl is also playing a role in the stabilization of the agostic structure. This means that Tp-agost-like species are in general not feasible intermediates; the structure Tp-agost seems to be only reliable for alkyneones with a phenyl group. In any event, it is not a crucial intermediate, because the reaction can also take place through π -alkyne complexes.

To sum up, the relative stability between η^1 -ketone and π -alkyne species in TpRu–alkyne complexes has been demonstrated, justifying the experimental detection of the η^1 -O-ketone adducts **5–8**. The geometry of the most stable vinylidene (**13b**) agrees with the experimental X-ray structure of **15**. A feasible pathway for the isomerization of the internal alkyne to the vinylidene has been found (route A-Tp), involving a 1,2-acyl direct shift from nondetected π -alkyne complexes and a Gibbs energy barrier (23.7 kcal mol⁻¹) very similar to the experimental barrier (23.5 kcal mol⁻¹). An alternative route from a η^2 -(C–C) agostic intermediate (C-Tp) which does not involve π -alkynes has also been described and cannot be discarded.

*Isomerization in the Cp*Ru Complex.* For the Cp*Ru complex, we have studied the three pathways described for the TpRu complex. The isomerization has been studied in methanol, the solvent used in the experiments. Scheme 9 shows all the calculated species and their relative Gibbs energies, taking as zero energy the separated [Cp*Ru(κ^2 P,N-P'Pr₂CH₂Py)]⁺ (**0-Cp***), Cl⁻, and PhC \equiv CCOMe (**A-alk**). The optimized structures of selected Cp* species relevant for the alkyne–vinylidene isomerization are shown in Figure 5. Table 8 collects structural data as well as charge distributions using NBO calculations.

According to theoretical calculations, the energy of chloride precursor **3** is quite similar to that of the separated species (**0-Cp*** + Cl⁻ + **A-alk**), in agreement with the spontaneous release of the halide in methanol solution. The π -alkyne intermediates (**9a,b**) are more stable than the separated species, both rotamers having

Scheme 9. Alkynone–Vinylidene Isomerization for Cp* Complexes **3**^a

^a $\Delta G_{\text{methanol}}$ values given in kcal mol⁻¹ with respect to the separated species.

similar energies, in agreement with the experimental detection of two rotamers in solution. Moreover, the energy of η^1 -keto alkyne intermediates ($\text{Cp}^*\text{-}\eta^1\text{-O}$) is too high to allow their detection in solution. The isomerization process takes place from the π -alkyne through a sigmatropic 1,2-shift of the acyl group. Two transition states similar to those of the TpRu system (Scheme 8) were located, $\text{TS}(9\mathbf{a} \rightarrow \text{Cp}^*\text{-vinyl}_\mathbf{a})$ and $\text{TS}(9\mathbf{b} \rightarrow \text{Cp}^*\text{-vinyl}_\mathbf{b})$ (routes A-Cp* and B-Cp*, respectively), depending on the π -alkyne rotamer. Starting from the corresponding π -alkyne species, **9a,b**, the activation barriers for each process are 32.7 and 28.8 kcal mol⁻¹, respectively. Both barriers for the isomerization in the Cp*Ru complex with a direct 1,2-acyl migration mechanism are notably higher than those for the TpRu complex (23.7 kcal mol⁻¹). An alternative route (C-Cp*) involving intermediate Cp*-agost, similar to Tp-agost, was investigated, but no such intermediate was located in the Cp*Ru complex. It appears that the possibility of a η^2 -(C-C) intermediate is limited to the TpRu complex with the PhC \equiv CCOME alkyne.

The calculated $\nu(\text{C}\equiv\text{C})$ absorptions for the two rotamers of **9** (**9a**, 1858 cm⁻¹; **9b**, 1839 cm⁻¹)³⁷ are in good agreement with the experimental IR $\nu(\text{C}\equiv\text{C})$ absorptions of complex **12** (1828 cm⁻¹) and are consistent with a strong π -bond/metal interaction. The C \equiv C distances in the Cp*- π -alkyne complexes (1.279 and 1.282 Å) are more elongated than in the

Tp- π -alkyne complexes (1.259 and 1.269 Å), suggesting a stronger π -bond/metal interaction in the Cp* complexes, as the π -alkyne binding energies to the unsaturated metal fragments **0-Tp** and **0-Cp*** confirm.

As for the Tp complex, in the Cp* system the increase of positive charge in the migratory group COMe (from reactant to transition state) substantiates the electrophilic nature of the process. The charge increase in C $_{\alpha}$ and the decrease in C $_{\beta}$ support this statement.

In conclusion, calculations confirm the capability of the Cp*Ru derivatives [$\text{Cp}^*\text{RuCl}(\kappa^2\text{P},\text{N}^1\text{Pr}_2\text{PXPpy})$] (X = CH₂ (**3**), NH (**4**)) to release the halide spontaneously and the calculations justify the nondetection of η^1 -O-ketone adducts. Both isomerization routes A-Cp* and B-Cp* demand too much energy, and they should not occur under standard reaction conditions. The π -alkyne complexes are the only accessible species in this system, in agreement with the experimental detection of complexes **9–11** and the nondetection of vinylidenes Cp*-vinyl.

*Ligand Effects in the Isomerization of Internal Alkynes: Tp vs Cp**. The Gibbs energy profiles depicted in Figure 6 describe the most favorable pathways for the isomerization of the internal alkyne PhC \equiv CCOME in the Tp and Cp* complexes in the solvent used in the experiments (fluorebenzene and methanol, respectively). Additional ΔG profiles comparing Cp* and Tp complexes using the same solvent have been included in the

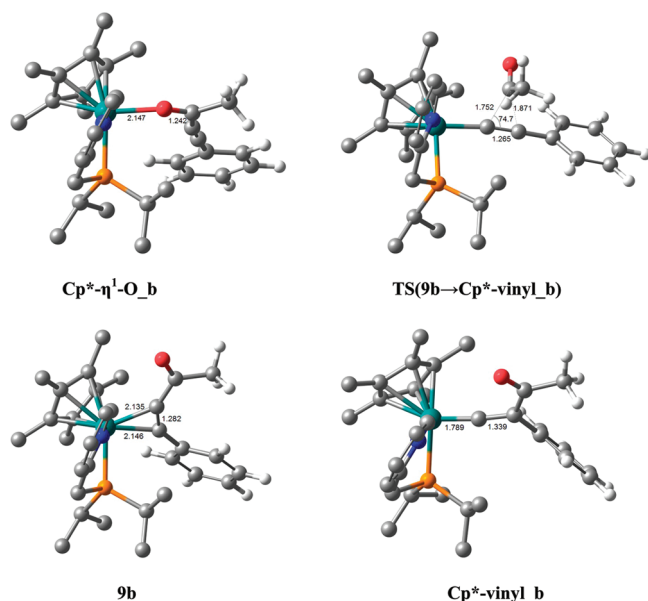


Figure 5. Optimized structures of selected species of the alkyne–vinylidene isomerization in the Cp*Ru complex. Bond distances are given in Å and angles in deg. Hydrogen atoms on Tp and P,N ligands have been removed for clarity.

Table 8. Structural and Electronic Changes along the 1,2-Acyl Migration in the Cp* Complex

		TS		TS
	9a	(9a→Cp*-vinyl_a)	9b	(9b→Cp*-vinyl_b)
$d(\text{C}(\text{O})-\text{C}_\alpha)$, Å	1.456	1.787	1.458	1.752
$d(\text{C}(\text{O})-\text{C}_\beta)$, Å	2.614	1.897	2.604	1.871
$d(\text{C}_\alpha-\text{C}_\beta)$, Å	1.279	1.265	1.282	1.265
$q(\text{COMe})$	-0.00	+0.18	-0.02	+0.12
$q(\text{C}_\alpha)$	-0.10	-0.01	-0.13	-0.02
$q(\text{C}_\beta)$	+0.06	-0.00	+0.08	+0.01

Supporting Information and show essentially the same behavior. The thermodynamics for the reaction from the separated species (**0-Tp** and **0-Cp***) are very similar in both systems, the vinylidene being in both cases about 12 kcal mol⁻¹ more stable. The most apparent features of the plots in Figure 6 are the different stabilities of η^1 -ketone and π -alkyne species in both systems and the differences in the barrier height for the 1,2-acyl migration. As the migratory aptitude of the substituent is the same in both systems because it is always a COMe acyl, the ligand (Tp or Cp*) decides the fate of the alkyne in the coordination sphere of the ruthenium. The increased stability of the π -alkyne combined with a higher barrier for its isomerization to vinylidene avoids the transformation in Cp*Ru complexes. In contrast, destabilization of the π -alkyne and a lower barrier for the isomerization of the internal alkyne allow vinylidene formation in TpRu complexes even for alkyne substituents with lower migration aptitude than acyls. The relative energy of the 1,2-acyl migration transition state with respect to the separated reactants is about 5 kcal mol⁻¹ lower for the TpRu complex, indicating better suitability of the TpRu fragment for stabilizing this TS.

To further analyze why the η^1 -O-ketone coordination mode is preferred with the Tp ligand and the π -alkyne is preferred with

the Cp* ligand, an energy decomposition analysis (EDA) was carried out to compare both coordination modes (Tables 9 and 10). The most stable isomers were selected for the study: Cp*- η^1 -O_a and **9a** as η^1 -O-ketone and π -alkyne complexes, respectively, in the Cp* system and **5b** (η^1 -O-ketone) and Tp- π -alk_b (π -alkyne) in the Tp system.

In the EDA the bonding energy (ΔE_b) between the unsaturated metal fragment [LRu(κ^2 P,N- $\text{Pr}_2\text{PCH}_2\text{Py}$)]⁺ (L = Tp, Cp*) and the alkyne in each coordination mode is decomposed into two main terms: one accounts for the distortion from their free geometries to those they adopt in the complexes (ΔE_{dist}), the other one concerns the interaction energy between the distorted fragments to form the complex structure (ΔE_{inter}). The latter in turn can be split into several contributions: ΔE_{Pauli} comprises the destabilizing interactions between occupied orbitals and is responsible for any steric repulsion; ΔE_{elst} corresponds to the classical electrostatic interaction; ΔE_{oi} accounts for electron pair bonding, charge transfer, and polarization.

$$\Delta E_b = \Delta E_{\text{dist}} + \Delta E_{\text{int}}$$

where

$$\Delta E_{\text{int}} = \Delta E_{\text{Pauli}} + \Delta E_{\text{elst}} + \Delta E_{\text{oi}}$$

Table 9 collects the different energy contributions of Cp*-related species. The distortion energy $\Delta\Delta E_{\text{dist}}$ favors the η^1 -ketone Cp*- η^1 -O_a over π -alkyne **9a** by 28.0 kcal mol⁻¹. According to $\Delta\Delta E_{\text{inter}}$, $\Delta\Delta E_{\text{Pauli}}$ also encourages coordination of the alkyne in a η^1 -ketone mode by 133.7 kcal mol⁻¹ but $\Delta\Delta E_{\text{elst}}$ and $\Delta\Delta E_{\text{oi}}$ terms support π -alkyne **9a** by 88.1 and 82.6 kcal mol⁻¹. The overall energy $\Delta\Delta E_b$ favors the π -alkyne coordination mode by 9.0 kcal mol⁻¹ due to strong electrostatic and orbital contributions.

For Tp complexes (Table 10), $\Delta\Delta E_{\text{dist}}$ shows the same trend as for Cp* analogues: i.e., η^1 -ketone **5b** is preferred over π -alkyne Tp- π -alk_b by 27.1 kcal mol⁻¹. $\Delta\Delta E_{\text{Pauli}}$ favors η^1 -ketone **5b** by 106.4 kcal mol⁻¹, whereas $\Delta\Delta E_{\text{elst}}$ and $\Delta\Delta E_{\text{oi}}$ terms encourage the π -alkyne bonding mode Tp- π -alk_b by 64.3 kcal mol⁻¹. The overall energy ΔE_b slightly favors η^1 -ketone coordination mode over the π -alkyne by 4.9 kcal mol⁻¹.

According to the aforementioned data, the driving force which decides the relative stability is the interaction contribution. For the Cp* system, ΔE_{inter} can counterbalance ΔE_{dist} to form a π -alkyne structure; for the Tp system the interaction is substantially reduced in the π -alkyne mode and increased in the η^1 -ketone mode.

When each coordination mode is compared for Tp and Cp* systems (Table 11), the distortion trend $\Delta\Delta E_{\text{dist}}$ is similar between both of them; Tp complexes are more stabilized than Cp* species by approximately 2–3 kcal mol⁻¹. Relating the interaction contribution in η^1 -ketone complexes, $\Delta\Delta E_{\text{inter}}$ favors Tp-**5b** by 6.8 kcal mol⁻¹. Although $\Delta\Delta E_{\text{Pauli}}$ prefers Cp*- η^1 -O_a, $\Delta\Delta E_{\text{elst}}$ and $\Delta\Delta E_{\text{oi}}$ favor Tp-**5b**. On the other hand, π -alkyne complexes show the opposite trend: Cp*-**9a** is preferred by 8.0 kcal mol⁻¹. $\Delta\Delta E_{\text{Pauli}}$ encourages Tp- π -alk_b, but this stabilization is canceled by electrostatic and orbital contributions.

These results show the influence of the ligands according to the coordination mode. Electrostatic and orbital contributions favor η^1 -ketone interaction in Tp complexes and π -alkyne interaction in Cp* complexes. The opposite trend occurs for the Pauli term. As an overall result, $\Delta\Delta E_b$ encourages η^1 -ketone formation in Tp complexes by 8.6 kcal mol⁻¹ and favors π -alkyne

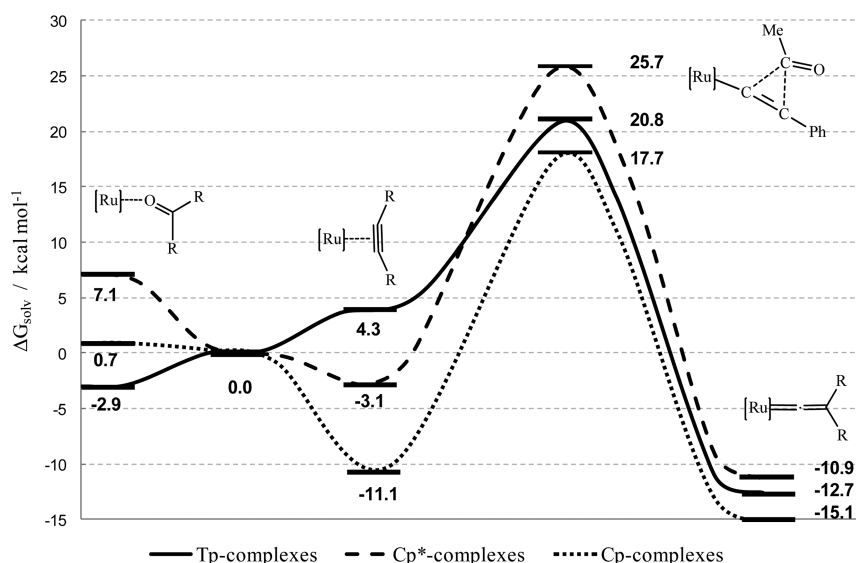


Figure 6. Gibbs energy profiles (kcal mol^{-1}) for the most favorable pathways for the isomerization of the internal alkyne $\text{PhC}\equiv\text{CCOMe}$ in the Tp (fluorebenzene solvent) and Cp^* complexes (methanol solvent). Results for the Cp complex in methanol are also included for comparison.

Table 9. Energy Decomposition Analysis for Cp^* Complexes^a

	$\Delta E_{\eta^1\text{-ketone}}(\text{Cp}^*\text{-}\eta^1\text{-O}_a)$	$\Delta E_{\pi\text{-alkyne}}(9a)$	$\Delta\Delta E^b$
$\Delta E_{\text{dist}}[\text{Cp}^*(\text{PN})\text{Ru}]^+$	5.4	11.6	-6.2
$\Delta E_{\text{dist}}(\text{PhCCCOMe})$	1.0	22.8	-21.8
ΔE_{dist}	6.4	34.4	-28.0
ΔE_{Pauli}	62.0	195.7	-133.7
ΔE_{elst}	-53.6	-141.7	88.1
ΔE_{oi}	-32.9	-115.5	82.6
ΔE_{inter}	-24.5	-61.5	37.0
ΔE_b	-18.1	-27.1	9.0

^a Gas-phase energies are given in kcal mol^{-1} . ^b $\Delta\Delta E = \Delta E(\eta^1\text{-ketone}) - \Delta E(\pi\text{-alkyne})$.

Table 10. Energy Decomposition Analysis for Tp Complexes^a

	$\Delta E_{\eta^1\text{-ketone}}(5b)$	$\Delta E_{\pi\text{-alkyne}}(\text{Tp-}\pi\text{-alk}_b)$	$\Delta\Delta E^b$
$\Delta E_{\text{dist}}[\text{Tp}(\text{PN})\text{Ru}]^+$	2.2	11.8	-9.6
$\Delta E_{\text{dist}}(\text{PhCCCOMe})$	2.4	19.9	-17.5
ΔE_{dist}	4.6	31.7	-27.1
ΔE_{Pauli}	68.8	175.2	-106.4
ΔE_{elst}	-61.6	-125.9	64.3
ΔE_{oi}	-38.5	-102.8	64.3
ΔE_{inter}	-31.3	-53.5	22.2
ΔE_b	-26.7	-21.8	-4.9

^a Gas-phase energies are given in kcal mol^{-1} . ^b $\Delta\Delta E = \Delta E(\eta^1\text{-ketone}) - \Delta E(\pi\text{-alkyne})$.

in Cp^* complexes by $5.3 \text{ kcal mol}^{-1}$. This means that the donor ability of the Cp^* ligand increases the electronic density on the metal, encouraging back-bonding in π -acceptor alkyne and, therefore, destabilizing σ -donor η^1 -ketone.

The reasons for the lower relative energy of the transition state in the Tp system are also apparent when the EDA is applied to

Table 11. Energy Decomposition Analysis Comparison between Tp and Cp^* Complexes^a

	$\Delta\Delta E$		
	$\eta^1\text{-ketone}$ ($\text{Cp}^*\text{-}\eta^1\text{-O}_a$)-5b	$\pi\text{-alkyne}$ 9a-(Tp- $\pi\text{-alk}_b$)	TS TS(9b-Cp*-vinyl_b)- TS(Tp- $\pi\text{-alk}_a$ -13a)
ΔE_{dist}	1.8	2.7	1.7
ΔE_{Pauli}	-6.8	20.5	13.4
ΔE_{elst}	8.0	-15.8	-3.3
ΔE_{oi}	5.6	-12.7	-6.2
ΔE_{inter}	6.8	-8.0	3.9
ΔE_b	8.6	-5.3	5.7

^a Gas-phase energies are given in kcal mol^{-1} .

both transition states (Table 11). In the Cp^*Ru complex the larger steric repulsion ($\Delta\Delta E_{\text{Pauli}} = 13.4 \text{ kcal mol}^{-1}$) cannot be counterbalanced by the electrostatic and orbital interactions, placing this transition state about 5 kcal mol^{-1} above that of the TpRu complex.

As previously reported complexes able to achieve the vinylidene formation bear Cp ligands,^{13–15} we wondered about the behavior that the hypothetical Cp complex $[\text{CpRuCl}(\kappa^2P, N^1\text{Pr}_2\text{PXPpy})]^+$ would exhibit. We have studied the isomerization of $\text{PhC}\equiv\text{CCOMe}$ in this complex, the main results being shown in Figure 6 (optimized structures collected in the Supporting Information). As expected, the relative energy of the transition state with respect to separated reactants is the lowest in the Cp complex ($17.7 \text{ kcal mol}^{-1}$, 8 kcal mol^{-1} lower than for the Cp^* complex). However, the π -alkyne intermediate is stabilized by the same amount, leading to almost the same barrier (28 kcal mol^{-1}) in both systems and thus hampering the isomerization also in this CpRu complex. Summing up, the isomerization of internal alkynes requires both stabilization of the transition state of the 1,2-migration and destabilization of the π -alkyne intermediate. The nature of the migrating group influences the transition state, but the nature of the metal ligands affects both the transition state and π -alkyne stabilities.

CONCLUSIONS

The participation of vinylidenes in the catalytic transformation of internal alkynes has been generally ruled out due to the consensus that internal alkynes did not isomerize to vinylidene. Reports by Shaw¹³ and Ishii et al.^{14,15} recently called our attention to this new field involving C–C activation by mononuclear ruthenium complexes.¹⁸

In this paper, we have completed the initial kinetic studies in solution and in the solid state. From an experimental point of view we have analyzed how the different modifications on the transition-metal ligands affect this transformation, namely (a) the pyridylphosphine linking group ($X = \text{NH}, \text{S}, \text{CH}_2$), (b) the alkyne substituents with and without ketone groups, and (c) the classical comparison between Cp- and Tp-type ligands (in this case between Cp*Ru and TpRu systems), in addition to the minor effect of the counterion (BPh₄ and B(Ar^F)₄) in Cp*Ru complexes.

In addition to the relatively important effects of modifications a and b on the isomerization rate of the TpRu– η^1 -O=C(R)C≡CPh intermediate into TpRu=C=C(Ph)COR, the most intriguing feature is the divergent behavior observed for the analogous Cp*Ru system, which yields stable π -alkyne complexes, not observed in most of the TpRu complexes (only as very minor products during the isomerization of some of them).¹⁸ The kinetic measurements, both in solution and in the solid state, are consistent with an intramolecular concerted mechanism via a sigmatropic 1,2-C shift.

A detailed computational study of the process, which explains the contrasting behavior of Cp*Ru, has been performed with the actual experimental complexes in order to analyze the mechanism, showing (a) the electrophilic nature of the acyl 1,2-shift, (b) the weaker metal– π -alkyne interaction in TpRu complexes destabilizing such intermediates, (c) the lower barrier for the isomerization in the TpRu complex, and (d) the good agreement between the calculated Gibbs activation energy and that determined experimentally by the kinetic measurements. Calculations on Cp*Ru show that π -alkyne complexes are the only accessible species, being more stable than η^1 -O-ketone adducts, due to the increased electrostatic and orbital interactions in the Cp*Ru system. The routes to vinylidene demand too much energy due to the large steric repulsion in the transition state of the migration.

In summary, the computational analysis of the internal alkyne to vinylidene isomerization in the coordination sphere of TpRu and Cp*Ru systems provides a sound explanation of a series of divergent experimental facts. The isomerization of internal alkynes requires both low-energy transition states for the 1,2-migration and destabilization of the π -alkyne intermediates. The nature of the metal ligands has impact on both factors. A better understanding of the factors controlling the process should lead to the design of suitable transition-metal systems able to reproduce this behavior in a reversible fashion.⁴² This would constitute a great step into the future catalytic transformations of internal alkynes.

EXPERIMENTAL SECTION

All synthetic operations were performed under dry dinitrogen or argon using conventional Schlenk techniques. Tetrahydrofuran, diethyl ether, and petroleum ether (boiling point range 40–60 °C) were obtained oxygen- and water-free from an Innovative Technology, Inc., solvent purification apparatus. Fluorobenzene, methanol, 1,2-dichloroethane, and other solvents were of anhydrous quality and were used as received. All solvents were deoxygenated immediately before use. The

ligands ⁱPr₂PCH₂Py,¹⁹ ⁱPr₂PNHpy, and ⁱPr₂PSPy⁴³ were respectively prepared as described in previous papers by our group, following suitable adaptations of published procedures.⁴⁴ The complexes [Cp*RuCl(κ^2 P, N-ⁱPr₂PXPy)] ($X = \text{CH}_2$ (3),¹⁹ NH (4)⁴³) and the NaB(Ar^F)₄ salt (Ar^F = 3,5-CF₃C₆H₃)⁴⁵ were synthesized according to reported methods. All internal alkynes were purchased from Aldrich and directly employed without further purification. IR spectra were recorded from Nujol mulls on a Perkin-Elmer FTIR Spectrum 1000 spectrophotometer. NMR spectra were recorded on Varian Inova 400 and 600 MHz and Varian Gemini 300 MHz equipment. Chemical shifts are given in parts per million from SiMe₄ (¹H and ¹³C{¹H}) or 85% H₃PO₄ (³¹P{¹H}). ¹H and ¹³C{¹H} NMR signal assignments were confirmed by ¹H-gCOSY, 13S-DEPT, and gHSQC(¹H–¹³C) experiments. ¹H and ¹³C{¹H} NMR signals corresponding to BPh₄ and B(Ar^F)₄ anions are omitted for clarity. Microanalysis was performed on a LECO CHNS-932 elemental analyzer at the Servicio Central de Ciencia y Tecnología, Universidad de Cádiz.

TpRuCl(κ^2 P,N-PⁱPr₂CH₂Py)] (1). The starting complex [TpRuCl(PPh₃)₂] (874 mg, 1 mmol) was suspended in 20 mL of toluene. After addition of 209 mg (1 mmol) of PⁱPr₂CH₂Py, the mixture was stirred at 65 °C over 16 h. Then, the suspension was warmed to room temperature and a solid was formed. The solvent was partially removed under vacuum, and petroleum ether (20 mL) was added to complete the precipitation, and the resulting yellow microcrystalline solid was filtered, washed with petroleum ether, and dried under vacuum.

Yield: 414 mg (74%). Anal. Calcd for C₂₁H₃₀BClN₇PRu: C, 45.1; H, 5.41. Found: C, 45.1; H, 5.43. IR (Nujol, cm⁻¹): $\nu(\text{BH})$ 2479, $\nu(\text{C}=\text{C})/\nu(\text{C}=\text{N})$ 1599. ¹H NMR (400 MHz, CD₂Cl₂, 298 K): δ 0.68, 1.24, 1.31, and 1.51 (m, 3H each, PCH(CH₃)₂), 1.83 and 3.48 (m, 1H each, PCH(CH₃)₂), 3.66 (dd, 1H, ²J_{HH} = 15.6 Hz, ²J_{HP} = 10.7 Hz, PCH^aH^b), 4.19 (dd, 1H, ²J_{HH} = 15.6 Hz, ²J_{HP} = 10.0 Hz, PCH^aH^b), 6.03 and 6.20 (t, 1H each, ³J_{HH} = 2.0 Hz, Tp), 6.28 (m, 1H, Tp), 6.39 (d, 1H, ³J_{HH} = 2.0 Hz, Tp), 6.83 (t, 1H, ³J_{HH} = 6.0 Hz, Py), 7.50 (m, 2H, Py), 7.75, 7.79, and 7.81 (d, 1H each, ³J_{HH} = 1.6 Hz, Tp), 7.77 (m, 2H, Tp), 7.92 (d, ³J_{HH} = 5.6 Hz, Py). ³¹P{¹H} NMR (161.89 MHz, CD₂Cl₂, 298 K): δ 77.4. ¹³C{¹H} NMR (100.58 MHz, CD₂Cl₂, 298 K): δ 18.53, 19.27, 19.71, and 19.94 (d, ²J_{CP} = 4.7 Hz, PCH(CH₃)₂), 25.24 (d, ¹J_{CP} = 15.5 Hz, PCH(CH₃)₂), 26.12 (d, ¹J_{CP} = 17.9 Hz, PCH(CH₃)₂), 38.03 (d, ¹J_{CP} = 22.0 Hz, PCH₂), 105.2, 105.7, and 105.9 (s, Tp), 121.6 (s, C⁵Py), 122.5 (d, ³J_{CP} = 8.7 Hz, C³Py), 142.5 and 145.8 (s, Tp), 143.9 (s, C⁴Py), 155.3 (s, C⁶Py), 166.2 (d, ²J_{CP} = 5.5 Hz, C²Py).

Synthesis of η^1 -O-Alkynyl-Ketone Complexes. In a typical preparation, a solution of complex 1 (0.15 g, 0.27 mmol) or 2 (0.15 g, 0.26 mmol) in 10 mL of fluorobenzene was treated with a slight excess of the corresponding internal alkyne (0.30 mmol: 46 μ L of 4-phenyl-3-butyn-2-one, 62 mg of diphenylpropynone), and NaBAR^F₄ (0.30 mmol, 266 mg). The reaction mixture was stirred in ice bath for 30 min in the case of the 4-phenyl-3-butyn-2-one derivatives 5 and 7, and for 2 h at room temperature for the diphenylpropynone complexes 6 and 8. The initial yellow solution slowly turns to darker colors ranging from green to violet. The mixture was then filtered through Celite to remove the NaCl salt, and the volatiles were removed under vacuum. The oily residue was washed with petroleum ether (2 \times 10 mL) and taken to dryness to yield the corresponding product as solids.

[TpRu(η^1 -O=C(Me)C≡CPh)](κ^2 P,N-PⁱPr₂CH₂Py)][BAR^F₄] (5). Yield: 310 mg (75%). Anal. Calcd for C₆₃H₅₀B₂F₂₄N₇OPRu: C 49.4, H 3.29; Found: C 49.4, H 3.28. IR (Nujol, cm⁻¹): $\nu(\text{BH})$ 2488, $\nu(\text{C}=\text{C})$ 2204, 2160, $\nu(\text{C}=\text{N})/\nu(\text{C}=\text{C})/\nu(\text{C}=\text{O})$ 1664, 1610, 1576. ¹H NMR (400 MHz, CDCl₃, 298 K): δ 0.81, 0.97, 1.28, and 1.37 (m, 3H each, PCH(CH₃)₂), 2.02 and 2.56 (m, 1H each, PCH(CH₃)₂), 2.27 (s, 3H, COCH₃), 3.80 (m, 2H, PCH₂), 6.07 and 6.22 (t, 1H each, ³J_{HH} = 2.0 Hz, Tp), 6.34 (br s, 1H, Tp), 6.44 (d, 1H, ³J_{HH} = 2.0 Hz, Tp), 7.03 (m, 1H, Py), 7.05 (d, 2H, ³J_{HH} = 7.6 Hz, Ph), 7.35 – 8.00 (m, 22H, Tp + Ph + BAR^F₄ + Py), 8.17 (d, 1H, ³J_{HH} = 5.8 Hz, Py). ³¹P{¹H} NMR

(161.89 MHz, CDCl₃, 298 K): δ 71.7 (s). ¹³C{¹H} NMR (150.81 MHz, CDCl₃, 283 K): δ 17.11, 18.04, 18.78, and 18.92 (s, PCH(CH₃)₂), 24.13 (d, ¹J_{CP} = 19.8 Hz, PCH(CH₃)₂), 26.33 (d, ¹J_{CP} = 21.3 Hz, PCH(CH₃)₂), 34.38 (s, CH₃CO), 35.10 (d, ¹J_{CP} = 21.4 Hz, PCH₂), 87.42 and 106.7 (s, C≡CPh), 106.3, 106.8, and 106.9 (s, Tp), 118.3 (s, C⁵Py), 120.0 – 138.0 (s, Ph + Tp + BAr^F₄ + Py), 141.7 and 146.2 (s, Tp), 144.3 (s, C⁴–Py), 154.8 (s, C⁶Py), 164.8 (d, ²J_{CP} = 4.3 Hz, C²Py), 198.3 (s, COCH₃).

Synthesis of η^2 -Alkyne Complexes. In a typical preparation, 0.15 g of complex **3** or **4** (0.31 mmol) was dissolved in 10 mL of methanol, in addition to a slight excess of the corresponding internal alkyne (0.35 mmol: 54 μ L of 4-phenyl-3-butyne-2-one, 72 mg of diphenylpropynone, 53 μ L of methyl phenylpropionate, 42 μ L of ethyl 2-butyrate), and NaBPh₄ (0.35 mmol, 120 mg). A yellow precipitate was immediately formed. The suspension was stirred for 10 min at room temperature. The mixture was filtered and the solid washed with small amounts of ethanol (<5 mL) and petroleum ether (2 \times 10 mL) and then taken to dryness to yield the corresponding products as orange-yellow microcrystalline solids.

[Cp^{*}Ru(η^2 -PhC≡CCOME)(κ^2 P,N-P'Pr₂CH₂Py)][BPh₄][−] (**9**). Yield: 262 mg (93%). Anal. Calcd for C₅₆H₆₃BNOPRu: C 74.0, H 6.99; Found: C 74.0, H 6.98. IR (Nujol, cm^{−1}): ν (η^2 -C≡C) 1828, ν (CO) 1644, ν (Ph) 1579 cm^{−1}. ¹H NMR (400 MHz, CD₂Cl₂, 298 K): Major product δ 0.51, 1.03, 1.45, and 1.76 (m, 3H each, PCH(CH₃)₂), 1.49 (d, ⁴J_{HP} = 1.3 Hz, 15H, C₅(CH₃)₅), 2.59 (s, 3H, COCH₃), 1.93 and 2.81 (m, 2H, PCH(CH₃)₂), 3.02 (dd, 1H, ²J_{HH} = 17 Hz, ²J_{HP} = 7.2 Hz, PCH^aH^b), 3.43 (dd, 1H, ²J_{HH} = 17 Hz, ²J_{HP} = 4.8 Hz, PCH^aH^b), 6.90 – 7.50 (m, 27 H, Ph + BPh₄ + Py), 7.57 (t, 1H, ³J_{HH} = 7.7 Hz, Ph), 8.02 (d, 1H, ³J_{HH} = 6.0 Hz, Py). ³¹P{¹H} NMR (161.9 MHz, CD₂Cl₂, 298 K): δ 66.4 (s, 15%) and 69.8 (s, 85%). ¹³C{¹H} NMR (75.4 MHz, CD₂Cl₂, 298 K): Major product δ 9.40 (s, C₅(CH₃)₅), 18.21 – 19.90 (m, PCH(CH₃)₂), 26.42 (d, ¹J_{CP} = 16.7 Hz, PCH(CH₃)₂), 29.51 (d, ¹J_{CP} = 26.0 Hz, PCH(CH₃)₂), 33.15 (s, CH₃CO), 37.92 (d, ¹J_{CP} = 22.5 Hz, PCH₂), 86.10 (d, ²J_{CP} = 9.6 Hz, C≡C), 98.80 (d, ²J_{CP} = 2.2 Hz, C₅(CH₃)₅), 116.8 (d, ²J_{CP} = 4.8 Hz, C≡C), 121.8 – 136.0 (s, Ph + BPh₄ + Py), 138.9 (s, *ipso*-Ph), 139.4 (s, C⁴-py), 157.8 (s, C⁶-py), 163.6 (d, ²J_{CP} = 5.8 Hz, C²-py), 190.9 (s, COCH₃).

Synthesis of Vinylidene Complexes. These complexes were prepared by the same procedure employed for their isomeric complexes **5** – **8**, but stirring the solution mixture during 1 h at 50 °C for the 4-phenyl-3-butyne-2-one derivatives **13** and **15**, and for 48 h at 50 °C in the case of the diphenylpropynone complex **14**. Compounds **16** – **18** were heated for 20 h at 75 °C. The workup yields the corresponding complexes as dark brown solids. Suitable X-ray single crystals of **14** have been grown by slow diffusion of petroleum ether into a diethylether solution of the complex at 4 °C.

[TpRu{C=C(COME)Ph}(κ^2 P,N-P'Pr₂CH₂Py)][BAr^F₄][−] (**13**). Yield: 303 mg (73%). Anal. Calcd for C₆₃H₅₀B₂F₂₄N₇OPRu: C, 49.4, H, 3.29. Found: C, 49.2, H, 3.25. IR (Nujol, cm^{−1}): ν (BH) 2497, ν (C=N)/ ν (C=C)/ ν (C=O) 1666, 1609, 1582, 1566. ¹H NMR (400 MHz, CDCl₃, 298 K): δ 0.62, 1.00, 1.27, and 1.37 (m, 3H each, PCHCH₃), 1.90 and 2.80 (m, 1H each, PCHCH₃), 1.84 (s, 3H, COCH₃), 3.72 (m, 2H, PCH₂), 6.15 and 6.19 (t, 1H each, ³J_{HH} = 2.0 Hz, Tp), 6.33 and 6.57 (br s, 1H each, Tp), 6.72 (d, 2H, ³J_{HH} = 7.2 Hz, Ph), 7.00–7.91 (m, 23H, Tp + Ph + B(Ar^F)₄ + Py), 8.51 (d, 1H, ³J_{HH} = 6.0 Hz, Py). ³¹P{¹H} NMR (161.89 MHz, CDCl₃, 298 K): δ 64.3 (s). ¹³C{¹H} NMR (75.45 MHz, CDCl₃, 298 K): δ 17.11 and 19.18 (both d, ²J_{CP} = 5.6 Hz, PCH(CH₃)₂), 17.49 and 18.63 (both s, PCH(CH₃)₂), 25.23 (d, ¹J_{CP} = 20.3 Hz, PCH(CH₃)₂), 28.56 (d, ¹J_{CP} = 26.9 Hz, PCH(CH₃)₂), 29.92 (s, CH₃CO), 36.38 (d, ¹J_{CP} = 27.4 Hz, PCH₂), 106.9, 107.3, and 107.4 (br s, Tp), 124.3 (s, C⁵Py), 124.6 (d, ³J_{CP} = 8.0 Hz, C³Py), 128.0 – 130.5 (s, Ph + B(Ar^F)₄), 131.8 (s, Ru=C=C), 136.4, 137.4, and 137.8 (s, Tp), 140.5 and 142.5 (s, Tp), 141.0 (s, C⁴Py), 147.1 (s, Tp), 153.3 (s, C⁶Py), 161.7 (d, ²J_{CP} = 3.8 Hz, C²Py), 196.6 (s, COCH₃), 357.3 (d, ²J_{CP} = 18.2 Hz, Ru=C).

Kinetics Studies of the Alkynyl Ketone to Vinylidene Isomerization. NMR samples of the alkynyl ketones **5**–**7** in 1,1,2,

2-tetrachloroethane-*d*₂ were prepared and immediately cooled to 213 K. The sample was warmed to room temperature just before being inserted into the probe of the Varian UNITY-400 spectrometer at 298 K. Once the shims were adjusted, the probe was heated to the desired temperature. The NMR temperature controller was previously calibrated against a methanol sample, the reproducibility being ± 1 °C. ³¹P{¹H} NMR spectra were recorded for at least 3 half-lives at regular intervals using the spectrometer software for accurate time control. Peak intensities were analyzed from stacked plots of the ³¹P{¹H} NMR spectra. First-order rate constants were derived from the least-squares best-fit lines of the ln(I₀/I_t) vs time plots (see the Supporting Information). The uncertainty in the isomerization rate constants represents the standard deviation derived from the slope of the best-fit line. Uncertainties in the activation enthalpies and entropies were calculated from the uncertainties in the slope and intercept of the best-fit lines of the Eyring plots and the error propagation formulas derived from the Eyring equation.

Kinetic Studies of the Alkynyl Ketone to Vinylidene Solid-State Isomerization. Solid samples of the alkynyl ketone **5** were prepared as Nujol mulls between two NaCl crystal windows. The samples were kept in an oven at the desired temperature (37, 45, and 50 °C). As each sample was taken out, the IR spectrum was recorded at room temperature, and then the sample was returned to the oven. The α (fraction of transformed solid) vs time curves were obtained by monitoring the decrease of the integrated intensity of the ν (C≡C) IR band for each compound as a function of time. The value α at a given *t* instant was calculated from: $\alpha(t) = (I_0 - I_t)/I_0$. Rate constants (*k*) and the values of *n* were derived from least-squares fits of ln(ln(1/(1 - α))) vs ln *t* plots (Avrami–Erofeev equation). The uncertainty in the value of *n* and in the isomerization rate constants represents 1 standard deviation, derived from the slope and the intercept of the best-fit lines.

Crystal Structure Analysis. Crystals of **2**, **12**, **15**, and **16** suitable for X-ray structural determination were mounted on glass fibers and then transferred to the cold nitrogen gas stream of a Bruker Smart APEX CCD three-circle diffractometer (*T* = 100 K) with a sealed-tube source and graphite-monochromated Mo K α radiation (λ = 0.710 73 Å) at the Servicio Central de Ciencia y Tecnología de la Universidad de Cádiz. In each case, four sets of frames were recorded over a hemisphere of the reciprocal space by ω scans with $\delta(\omega) = 0.30^\circ$ and an exposure of 10 s per frame. Correction for absorption was applied by scans of equivalents using the SADABS program.⁴⁶ An insignificant crystal decay correction was also applied. The structures of **2**, **12**, and **16** were solved by direct methods. The structure of **15** was solved by vectorial methods. All the structures were refined on *F*² by full-matrix least squares (SHELX97)⁴⁷ by using all unique data. All non-hydrogen atoms were refined anisotropically with hydrogen atoms included in calculated positions (riding model). Three disordered CF₃ groups in compound **16** were refined split in two complementary orientations using displacement parameter restraints. The program ORTEP-3 was used for plotting.⁴⁸

Table 12 summarizes the crystal data and data collection and refinement details for **2**, **12**, **15**, and **16**. An ORTEP diagram of **2** can be found in the Supporting Information. CCDC 815989–815992 contain supplementary crystallographic data for this paper. These data can be obtained free of charge from The Cambridge Crystallographic Data Centre via www.ccdc.cam.ac.uk/data_request/cif.

Computational Details. All calculations were performed at the DFT level by means of the PBE0 functional⁴⁹ as implemented in Gaussian 09.⁵⁰ This functional correctly described the uniform electron gas (UEG) limit, which accurately reproduces agostic bonding situations.⁵¹ Test calculations were performed with the M06 functional.⁵² The Ru atom was described using the scalar-relativistic Stuttgart–Dresden SDD pseudopotential⁵³ and its associated double- ζ basis set complemented with a set of *f*-polarization functions.⁵⁴ The 6-31G** basis set was used for the H⁵⁵ and B, C, N, O, P, and Cl atoms.⁵⁶ Diffuse functions were added for O and Cl atoms⁵⁷ in all calculations. Solvent effects were

Table 12. Crystal Data and Details of the Structure Determination of Compounds 2, 12, 15, and 16

	2	12	15	16	
		Crystal Data			
formula	C ₂₀ H ₂₈ BClN ₇ PRuS	C ₃₆ H ₄₄ N ₂ OPRu, C ₂₄ H ₂₀ B	C ₃₀ H ₃₆ BN ₇ OPRuS, C ₃₂ H ₁₂ BF ₂₄	C ₃₀ H ₃₇ BN ₈ O ₂ PRu, C ₃₂ H ₁₂ BF ₂₄	
formula wt	576.86	971.98	1548.79	1547.75	
cryst syst	monoclinic	triclinic	triclinic	triclinic	
space group	<i>P</i> 2 ₁ / <i>c</i> (No. 14)	<i>P</i> $\bar{1}$ (No. 2)	<i>P</i> $\bar{1}$ (No. 2)	<i>P</i> $\bar{1}$ (No. 2)	
<i>a</i> , Å	30.334(6)	13.599(3)	11.765(2)	12.484(3)	
<i>b</i> , Å	10.568(2)	13.869(3)	16.274(3)	13.946(3)	
<i>c</i> , Å	15.019(3)	13.899(3)	18.114(4)	20.184(4)	
α , deg	90.00	70.76(3)	87.45(3)	74.11(3)	
β , deg	92.76(3)	84.98(3)	71.52(3)	77.51(3)	
γ , deg	90.00	89.92(3)	79.53(3)	85.73(3)	
<i>V</i> , Å ³	4809.1(16)	2464.5(10)	3234.2(13)	3299.4(14)	
<i>Z</i>	8	2	2	2	
<i>D</i> _{calcd} , g/cm ³	1.594	1.310	1.590	1.557	
μ (Mo K α), mm ⁻¹	0.940	0.394	0.417	0.380	
<i>F</i> (000)	2352	1020	1556	1556	
dryst size, mm	0.04 × 0.52 × 0.56	0.13 × 0.16 × 0.35	0.36 × 0.54 × 0.62	0.35 × 0.42 × 0.54	
		Data Collection			
temp, K	100	100	100	100	
radiation (λ , Å)	Mo K α (0.71073)	Mo K α (0.71073)	Mo K α (0.71073)	Mo K α (0.71073)	
min, max θ , deg	0.7, 25.00	1.8, 25.0	1.8, 27.5	1.1, 27.5	
data set	−36 to +33; −12 to +12; −17 to +17	−16: to +13; −16 to +16; −16 to +16	−15 to +15; −21 to +20; −21 to +23	−16 to +14; −18 to +18; −26 to +26	
total, unique no. of data; <i>R</i> (int)	29 934, 8374; 0.076	17 485, 8603; 0.023	27 453, 14 466; 0.017	27 367, 14 711; 0.014	
no. of obsd data (<i>I</i> > 2.0 σ_I)	6835	8237	13 661	13 867	
		Refinement			
<i>N</i> _{ref} <i>N</i> _{param}	8374, 585	8603, 604	14 466, 897	14 711, 936	
<i>R</i> ₁ , <i>wR</i> ₂ , <i>S</i>	0.0625, 0.1295, ^a 1.07	0.0381, 0.0854, ^b 1.04	0.0371, 0.0922, ^c 1.04	0.0428, 0.1094, ^d 1.02	
max, av shift/error	0.00, 0.00	0.00, 0.00	0.00, 0.00	0.00, 0.00	
min, max resd dens, e Å ⁻³	−0.48, 1.00	0.45, 0.65	−0.58, 0.81	−0.91, 1.46	
^a $w = 1/[\sigma^2(F_o^2) + (0.0492P)^2 + 14.3646P]$, where $P = (F_o^2 + 2F_c^2)/3$. ^b $w = 1/[\sigma^2(F_o^2) + (0.0312P)^2 + 3.1323P]$, where $P = (F_o^2 + 2F_c^2)/3$. ^c $w = 1/[\sigma^2(F_o^2) + (0.0435P)^2 + 2.929P]$, where $P = (F_o^2 + 2F_c^2)/3$. ^d $w = 1/[\sigma^2(F_o^2) + (0.0537P)^2 + 5.2586P]$, where $P = (F_o^2 + 2F_c^2)/3$.					

introduced through CPCM⁵⁸ single-point calculations on gas-phase optimized geometries. The solvents employed in the experiments (fluorobenzene, $\epsilon = 5.42$; methanol, $\epsilon = 32.61$) were described with this continuum method. The structures of the reactants, intermediates, transition states, and products were fully optimized without any symmetry restriction. Transition states were identified by having one imaginary frequency in the Hessian matrix. It was confirmed that transition states connect with the corresponding intermediates by means of application of an eigenvector corresponding to the imaginary frequency and subsequent optimization of the resulting structures. Gibbs energies in solution at 298 K (ΔG_{solv}) were obtained from adding the gas-phase Gibbs energy corrections of the solute to ΔE_{solv} as indicated below,⁵⁹ where “gp” means gas-phase calculations:

$$\Delta G_{\text{solv}} = \Delta E_{\text{solv}} + (\Delta G_{\text{gp}} - E_{\text{gp}})$$

Natural bond orbital (NBO) analysis was performed with NBO Version 3.1⁶⁰ incorporated in the Gaussian 09 package. Binding interactions in selected complexes were analyzed using the energy-decomposition analysis⁶¹ with PBE0 functional as implemented in ADF-2009.⁶² According to this set of calculations, scalar relativistic effects

were considered using the ZORA formalism⁶³ and TZP (core double- ζ , valence triple- ζ , polarized) basis set⁶⁴ was used for all atoms.

■ ASSOCIATED CONTENT

Supporting Information. Text giving synthesis and characterization details of η^1 -*O*-alkynyl ketone, η^2 -alkyne, and vinylidene complexes, CIF files, figures giving $\ln(I_0/I_t)$ vs time and Eyring plots for isomerizations in solution, α vs time and $\ln(-\ln(1/(1-\alpha)))$ vs $\ln t$ plots for the isomerizations in the solid state, and an ORTEP view of the structure of compound 2, tables giving Cartesian coordinates, absolute energies, and Gibbs energies (hartrees) of all the optimized structures, and figures giving optimized structures of selected species of the alkynone–vinylidene isomerization in the CpRu complex. This material is available free of charge via the Internet at <http://pubs.acs.org>.

■ AUTHOR INFORMATION

Corresponding Author

*E-mail: pedro.valerga@uca.es (P.V.); agusti@klingon.uab.es (A.L.).

ACKNOWLEDGMENT

We thank the Spanish MICINN (Projects CTQ2010-15390, V.K.S. sabbatical leave SB2005-0124, CTQ2008-06866-C02-01, and ORFEO Consolider-Ingenio 2010 CSD2007-00006) and "Junta de Andalucía" (PAI - FQM188 and Project of Excellence PAI05 FQM094 - Project of Excellence P08-FQM-03538) for financial support and for a postdoc contract to E.B. and Johnson Matthey plc for generous loans of ruthenium trichloride. M.A.O. acknowledges the Spanish MICINN for an FPU fellowship.

REFERENCES

- (1) (a) Selegue, J. P. *Coord. Chem. Rev.* **2004**, *248*, 1543–1563. (b) Bruce, M. I. In *Metal Vinylidenes and Allenylidenes in Catalysis*; Bruneau, C., Dixneuf, P. H., Eds.; Wiley-VCH: Weinheim, Germany, 2008; pp 1–60.
- (2) Lynam, J. M. *Chem. Eur. J.* **2010**, *16*, 8238–8247.
- (3) (a) Trost, B.; McClory, A. *Chem. Asian J.* **2008**, *3*, 164–194. (b) Odedra, A.; Liu, R.-S. In *Metal Vinylidenes and Allenylidenes in Catalysis*; Bruneau, C., Dixneuf, P. H., Eds.; Wiley-VCH: Weinheim, Germany, 2008; pp 193–214. (c) Bruneau, C.; Dixneuf, P. H. *Angew. Chem., Int. Ed.* **2006**, *45*, 2176–2203. (d) Trost, B.; Frederiksen, M. U.; Rudd, M. T. *Angew. Chem., Int. Ed.* **2005**, *44*, 6630–6666.
- (4) (a) García-Yebra, C.; López-Mardomingo, C.; Fajardo, M.; Antiñolo, A.; Otero, A.; Rodríguez, A.; Vallat, A.; Luca, D.; Mugnier, Y.; Carbó, J. J.; Lledós, A.; Bo, C. *Organometallics* **2000**, *19*, 1749–1765. (b) Wakatsuki, Y. *J. Organomet. Chem.* **2004**, 4092–4109. (c) De Angelis, F.; Sgamellotti, A.; Re, N. *Dalton Trans.* **2004**, 3225–3230. (d) De Angelis, F.; Sgamellotti, A.; Re, N. *Organometallics* **2007**, *26*, 5285–5288. (e) Bassetti, M.; Cadierno, V.; Gimeno, J.; Pasquini, C. *Organometallics* **2008**, *27*, 5009–5016. (f) Zhu, J.; Lin, Z. In *Metal Vinylidenes and Allenylidenes in Catalysis*; Bruneau, C., Dixneuf, P. H., Eds.; Wiley-VCH: Weinheim, Germany, 2008; pp 129–157. (g) Cabeza, J. A.; Pérez-Carreño, E. *Organometallics* **2010**, *29*, 3973–3978. (h) Grotjahn, D. B.; Zeng, X.; Cooksy, A. L.; Kassel, W. S.; DiPasquale, A. G.; Zakharov, L. N.; Rheingold, A. L. *Organometallics* **2007**, *26*, 3385–3402. (i) Vastine, B. A.; Hall, M. B. *Organometallics* **2008**, *27*, 4325–4333.
- (5) Bustelo, E.; Carbo, J. J.; Lledós, A.; Mereiter, K.; Puerta, M. C.; Valerga, P. *J. Am. Chem. Soc.* **2003**, *125*, 3311–3321.
- (6) Puerta, M. C.; Valerga, P. *Coord. Chem. Rev.* **1999**, 193–195, 977–1025.
- (7) Bly, R. S.; Zhong, Z.; Kane, C.; Bly, R. K. *Organometallics* **1994**, *13*, 899–905.
- (8) (a) Werner, H.; Baum, M.; Schneider, D.; Windmüller, B. *Organometallics* **1994**, *13*, 1089–1097. (b) Connelly, N. G.; Geiger, W. E.; Lagunas, M. C.; Metz, B.; Rieger, A. L.; Rieger, P. H.; Shaw, M. J. *J. Am. Chem. Soc.* **1995**, *117*, 12202–12208. (c) Katayama, H.; Onitsuka, K.; Ozawa, F. *Organometallics* **1996**, *15*, 4642–4645. (d) Werner, H.; Lass, R. W.; Gevert, O.; Wolf, J. *Organometallics* **1997**, *16*, 4077–4088. (e) Jiménez, M. V.; Sola, E.; Lahoz, F. J.; Oro, L. A. *Organometallics* **2005**, *24*, 2722–2729. (f) Ilg, K.; Paneque, M.; Poveda, M. L.; Rendón, N.; Santos, L. L.; Carmona, E.; Mereiter, K. *Organometallics* **2006**, *25*, 2230–2236.
- (9) (a) Baum, M.; Mahr, N.; Werner, H. *Chem. Ber.* **1994**, *127*, 1877–1886. (b) Venkatesan, K.; Blacque, O.; Fox, T.; Alfonso, M.; Schmalte, H. W.; Berke, H. *Organometallics* **2004**, *23*, 1183–1186. (c) Venkatesan, K.; Blacque, O.; Fox, T.; Alfonso, M.; Schmalte, H. W.; Kheradmandan, S.; Berke, H. *Organometallics* **2005**, *24*, 920–932.
- (10) Miura, T.; Iwasawa, N. *J. Am. Chem. Soc.* **2002**, *124*, 518–519.
- (11) Millert, D. C.; Angelici, R. J. *Organometallics* **1991**, *10*, 81–89.
- (12) King, P. J.; Knox, S. A. R.; Legge, M. S.; Orpen, A. G.; Wilkinson, J. N.; Hill, E. A. *Dalton Trans.* **2000**, 1547–1548.
- (13) Shaw, M. J.; Bryant, S. W.; Rath, N. *Eur. J. Inorg. Chem.* **2007**, 3943–3946.
- (14) Ikeda, Y.; Yamaguchi, T.; Kanao, K.; Kimura, K.; Kamimura, S.; Mutoh, Y.; Tanabe, Y.; Ishii, Y. *J. Am. Chem. Soc.* **2008**, *130*, 16856–16857.
- (15) Mutoh, Y.; Ikeda, Y.; Kimura, K.; Ishii, Y. *Chem. Lett.* **2009**, *38*, 534–535.
- (16) (a) Gelabert, R.; Moreno, M.; Lluch, J. M.; Lledós, A. *Organometallics* **1997**, *16*, 3805–3814. (b) Jia, G.; Lau, C. P. *Coord. Chem. Rev.* **1999**, *190–192*, 83–108. (c) Man, M. L.; Zhu, J.; Ng, S. M.; Zhou, Z. Y.; Yin, C. Q.; Lin, Z. Y.; Lau, C. P. *Organometallics* **2004**, *23*, 6214–6220.
- (17) Besora, M.; Vyboishchikov, S. F.; Lledós, A.; Maseras, F.; Carmona, E.; Poveda, M. L. *Organometallics* **2010**, *29*, 2040–2045.
- (18) de los Ríos, I.; Bustelo, E.; Puerta, M. C.; Valerga, P. *Organometallics* **2010**, *29*, 1740–1749.
- (19) Jiménez-Tenorio, M.; Puerta, M. C.; Valerga, P.; Moncho, S.; Ujaque, G.; Lledós, A. *Inorg. Chem.* **2010**, *49*, 6035–6057.
- (20) Huang, Y.-H.; Gladysz, J. A. *J. Chem. Educ.* **1988**, *65*, 298–303.
- (21) Gemel, C.; LaPensee, A.; Mauthner, K.; Mereiter, K.; Schmid, R.; Kirchner, K. *Monatsh. Chem.* **1997**, *128*, 1189–1199.
- (22) (a) Reger, D. L.; Klaeren, S. A.; Lebioda, L. *Organometallics* **1988**, *7*, 189–193. (b) Ciardi, C.; Reginato, G.; Gonsalvi, L.; de los Ríos, I.; Romerosa, A.; Peruzzini, M. *Organometallics* **2004**, *23*, 2020–2026.
- (23) Orpen, A. G.; Brammer, L.; Allen, F. H.; Kennard, O.; Watson, D. G.; Taylor, R. *J. Chem. Soc., Dalton Trans.* **1989**, S1.
- (24) Manna, J.; John, K. D.; Hopkins, M. D. *Adv. Organomet. Chem.* **1995**, *38*, 79–154.
- (25) Lompfrey, J. R.; Selegue, J. P. *J. Am. Chem. Soc.* **1992**, *114*, 5518–5523.
- (26) O'Connor, J. M.; Friese, S. J.; Rodgers, B. L.; Rheingold, A. L.; Zakharov, L. *J. Am. Chem. Soc.* **2005**, *127*, 9346–9347.
- (27) Older, C. M.; Stryker, J. M. *Organometallics* **2000**, *19*, 2661–2663.
- (28) Jeffery, J. C.; Jelliss, P. A.; Psillakis, E.; Rudd, G. E. A.; Stone, F. G. A. *J. Organomet. Chem.* **1998**, 17–27.
- (29) Urtel, K.; Frick, A.; Huttner, G.; Zsolnai, L.; Kirchner, P.; Rutsch, P.; Kaifer, E.; Jacobi, A. *Eur. J. Inorg. Chem.* **2000**, 33–50.
- (30) (a) Bruce, M. I. *Chem. Rev.* **1991**, *91*, 197–257. (b) Silvestre, J.; Hoffmann, R. *Helv. Chim. Acta* **1985**, *68*. (c) Koga, N.; Yamazaki, H.; Morokuma, K. *J. Am. Chem. Soc.* **1994**, *116*, 8105–8111. (d) Grotjahn, D. B.; Miranda-Soto, V.; Kragulj, E. J.; Lev, D. A.; Erdogan, G.; Zeng, X.; Cooksy, A. L. *J. Am. Chem. Soc.* **2008**, *130*, 20–21.
- (31) Becker, E.; Pavlik, S.; Kirchner, K. *Adv. Organomet. Chem.* **2008**, *56*, 155–197 and references therein.
- (32) (a) Alkyne to vinylidene isomerization of $[\text{CpRu}(\eta^2\text{-HC}\equiv\text{CMe})\text{-}(\text{PMe}_3)_2][\text{PF}_6]$ ($\Delta H^\ddagger = 23.4 \text{ kcal mol}^{-1}$, $\Delta S^\ddagger = 3.9 \text{ cal mol}^{-1} \text{ K}^{-1}$): Bullock, R. M. *J. Chem. Soc., Chem. Commun.* **1989**, 165–167. (b) Vinylidene to alkyne isomerization of $[\text{CpMo}(=\text{C}=\text{CH}^t\text{Bu})(\text{CO})(\text{NO})]$ ($\Delta H^\ddagger = 29.0 \text{ kcal mol}^{-1}$, $\Delta S^\ddagger = 1.8 \text{ cal mol}^{-1} \text{ K}^{-1}$): Ipaktschi, J.; Mohsseni-Ala, J.; Uhlig, S. *Eur. J. Inorg. Chem.* **2003**, 4313–4320. (c) Release of terminal alkynes from indenylruthenium vinylidene complexes ($\Delta H^\ddagger = 24 \text{ kcal mol}^{-1}$, $\Delta S^\ddagger = -3 \text{ cal mol}^{-1} \text{ K}^{-1}$): ref 4e.
- (33) Spangler, C. W. *Chem. Rev.* **1976**, *76*, 187–217 and references therein.
- (34) Wang, Y.; Agbossou, F.; Dalton, D. M.; Liu, Y.; Arim, A. M.; Gladysz, J. A. *Organometallics* **1993**, *12*, 2699–2713.
- (35) Solid-state reactions can be described by equations of the type $F(\alpha) = kt$, where the function $F(\alpha)$ depends on the reaction-controlling mechanism, as well as the size and shape of the reacting particles. This type of conversion function may be described in terms of the reaction-rate-controlling Avrami–Erofeev model, by the general formula $\alpha = 1 - \exp(-kt^n)$, where n is empirically determined via a fitting procedure. The Avrami exponent is indicative of the reaction mechanism and crystal growth dimensions: (a) Avrami, M. *J. Chem. Phys.* **1939**, *7*, 1103–1112. (b) Avrami, M. *J. Chem. Phys.* **1940**, *8*, 212–224. (c) Avrami, M. *J. Chem. Phys.* **1941**, *9*, 177–184.
- (36) Haber, J.; Jamroz, K. *J. Solid State Chem.* **1982**, *44*, 291–297.
- (37) (a) The scaling factor of 0.9536 recommended in ref 37b for the vibrational frequencies calculated with the employed combination of exchange-correlation functional and basis set has been applied.

(b) Tantirungrotechai, Y.; Phanasant, K.; Roddecha, S.; Surawatana-wong, P.; Sutthikhum, V.; Limtrakul, J. *J. Mol. Struct. (THEOCHEM)* **2006**, *760*, 189–192.

(38) We have not been able to find a nondissociative transition state for the η^1 -O-ketone \rightarrow π -alkyne interconversion despite performing an extensive search.

(39) De Angelis, F.; Sgamellotti, A.; Re, N. *Organometallics* **2002**, *21*, 5944–5950.

(40) (a) Ujaque, G.; Maseras, F.; Lledós, A.; Contreras, L.; Pizzano, A.; Rodewald, D.; Sánchez, L.; Carmona, E.; Monge, A.; Ruiz, C. *Organometallics* **1999**, *18*, 3294–3305. (b) Jaffart, J.; Etienne, M.; Reinhold, M.; McGrady, J. E.; Maseras, F. *Chem. Commun.* **2003**, 876–877. (c) Boulho, C.; Keys, T.; Coppel, Y.; Vendier, L.; Etienne, M.; Locati, A.; Bessac, F.; Maseras, F.; Pantazis, D. A.; McGrady, J. E. *Organometallics* **2009**, *28*, 940–943. (d) Etienne, M.; McGrady, J. E.; Maseras, F. *Coord. Chem. Rev.* **2009**, *253*, 635–646.

(41) We have not been able to locate a transition state connecting **Tp-agost** with the π -alkyne complex, but small distortions on the geometry of **Tp-agost** lead directly to the π -alkyne, indicating that it should be a shallow minimum.

(42) In a recent communication, the first example of a reversible disubstituted vinylidene-to-internal alkyne isomerization on reaction with a monophosphine has been shown: Mutoh, Y.; Imai, K.; Kimura, Y.; Ikeda, Y.; Ishii, Y. *Organometallics* **2011**, *30*, 204–207. We have checked this possibility with one of our vinylidene systems, and this also confirmed the release of the alkyne upon treatment with triphenylphosphine and heating.

(43) Macías-Arce, I.; Puerta, M. C.; Valerga, P. *Eur. J. Inorg. Chem.* **2010**, 1767–1776.

(44) Jansen, A.; Pitter, S. *Monatsh. Chem.* **1999**, *130*, 783–794.

(45) Brookhart, M.; Grant, B.; Volpe, A. F. *Organometallics* **1992**, *11*, 3920–3922.

(46) Sheldrick, G. M. *SADABS, 2001 version*; University of Göttingen, Göttingen, Germany, 2001.

(47) (a) Sheldrick, G. M. *SHELXTL version 6.10, Crystal Structure Analysis Package*; Bruker AXS, Madison, WI, 2000. (b) Sheldrick, G. M. *Acta Crystallogr.* **2008**, *A64*, 112–122.

(48) Farrugia, L. J. ORTEP-3 for Windows, version 1.076. *J. Appl. Crystallogr.* **1997**, *30*, 565.

(49) (a) Perdew, J. P.; Burke, K.; Ernzerhof, M. *Phys. Rev. Lett.* **1996**, *77*, 3865–3868. (b) Perdew, J. P.; Ernzerhof, M.; Burke, K. *J. Chem. Phys.* **1996**, *105*, 9982–9985.

(50) Frisch, M. J.; Trucks, G. W.; Schlegel, H. B.; Scuseria, G. E.; Robb, M. A.; Cheeseman, J. R.; Scalmani, G.; Barone, V.; Mennucci, B.; Petersson, G. A.; Nakatsuji, H.; Caricato, M.; Li, X.; Hratchian, H. P.; Izmaylov, A. F.; Bloino, J.; Zheng, G.; Sonnenberg, J. L.; Hada, M.; Ehara, M.; Toyota, K.; Fukuda, R.; Hasegawa, J.; Ishida, M.; Nakajima, T.; Honda, Y.; Kitao, O.; Nakai, H.; Vreven, T.; Montgomery, J. A., Jr.; Peralta, J. E.; Ogliaro, F.; Bearpark, M.; Heyd, J. J.; Brothers, E.; Kudin, K. N.; Staroverov, V. N.; Kobayashi, R.; Normand, J.; Raghavachari, K.; Rendell, A.; Burant, J. C.; Iyengar, S. S.; Tomasi, J.; Cossi, M.; Rega, N.; Millam, J. M.; Klene, M.; Knox, J. E.; Cross, J. B.; Bakken, V.; Adamo, C.; Jaramillo, J.; Gomperts, R.; Stratmann, R. E.; Yazyev, O.; Austin, A. J.; Cammi, R.; Pomelli, C.; Ochterski, J. W.; Martin, R. L.; Morokuma, K.; Zakrzewski, V. G.; Voth, G. A.; Salvador, P.; Dannenberg, J. J.; Dapprich, S.; Daniels, A. D.; Ö. Farkas, Foresman, J. B.; Ortiz, J. V.; Cioslowski, J.; Fox, D. J. *Gaussian 09, Revision A.1*; Gaussian, Inc., Wallingford, CT, 2009.

(51) Pantazis, D. A.; McGrady, J. E.; Besora, M.; Maseras, F.; Etienne, M. *Organometallics* **2008**, *27*, 1128–1134.

(52) Zhao, Y.; Truhlar, D. G. *Theor. Chem. Acc.* **2008**, *120*, 215–241.

(53) Andrae, D.; Haeussermann, U.; Dolg, M.; Stoll, H.; Preuss, H. *Theor. Chim. Acta* **1990**, *77*, 123–141.

(54) Ehlers, A. W.; Bohme, M.; Dapprich, S.; Gobbi, A.; Hollwarth, A.; Jonas, V.; Kohler, K. F.; Stegmann, R.; Veldkamp, A.; Frenking, G. *Chem. Phys. Lett.* **1993**, *208*, 111–114.

(55) Hehre, W. J.; Ditchfield, R.; Pople, J. A. *J. Chem. Phys.* **1972**, *56*, 2257–2261.

(56) Francl, M. M.; Pietro, W. J.; Hehre, W. J.; Binkley, J. S.; Gordon, M. S.; DeFrees, D. J.; Pople, J. A. *J. Chem. Phys.* **1982**, *77*, 3654–3665.

(57) Clark, T.; Chandrasekhar, J.; Spitznagel, G. W.; Schleyer, P. v. R. *J. Comput. Chem.* **1983**, *4*, 294–301.

(58) Cossi, M.; Rega, N.; Scalmani, G.; Barone, V. *J. Comput. Chem.* **2003**, *24*, 669–681.

(59) Braga, A. A. C.; Ujaque, G.; Maseras, F. *Organometallics* **2006**, *25*, 3647–3658.

(60) Glendening, E. D.; Reed, A. E.; Carpenter, J. E.; Weinhold, F. *NBO Version 3.1*.

(61) (a) Kitaura, K.; Morokuma, K. *Int. J. Quantum Chem.* **1976**, *10*, 325–340. (b) Ziegler, T.; Rauk, A. *Theor. Chim. Acta* **1977**, *46*, 1–10.

(62) *ADF2009, SCM*; Theoretical Chemistry, Vrije Universiteit, Amsterdam, The Netherlands, <http://www.scm.com>.

(63) (a) van Lenthe, E.; Baerends, E. J.; Snijders, J. G. *J. Chem. Phys.* **1994**, *101*, 9783–9792. (b) van Lenthe, E.; Ehlers, A.; Baerends, E. J. *J. Chem. Phys.* **1999**, *110*, 8943–8953.

(64) van Lenthe, E.; Baerends, E. J. *J. Comput. Chem.* **2003**, *24*, 1142–1156.